*Mathematical Biosciences and Engineering*

https://www.aimspress.com/journal/mbe

MBE, 23(9): 2655–2697.
DOI: 10.3934/mbe.2026096
Received: 23 February 2026
Revised: 20 July 2026
Accepted: 05 August 2026
Published: 07 September 2026

*Research article*

# Coupled Pest–disease dynamics and cacao losses: A mathematical modeling approach

**Myriam Djoukwe Tapi** [1,2,3,4,*], **Nico Stollenwerk** [4], **Samuel Bowong** [1,2,3] **and Maíra Aguiar** [4,5]

[1] Department of Mathematics and Computer Science, Faculty of Science, The University of Douala, PO Box 24157 Douala

[2] IRD, Sorbonne University, UMMISCO, F-93143, Bondy, France

[3] EPITAG project, MACBES, Sophia Antipolis, France

[4] Basque Center for Applied Mathematics, Alameda de Mazarredo 14, Bilbao, E-48009, Basque Country, Spain

[5] Ikerbasque, Basque Foundation for Science, Bilbao, Spain

* **Correspondence:** Email: myriamtapi@yahoo.fr/mdjoukwe@bcamath.org; Tel: +237-677-55-3068.

**Abstract:** Black pod disease and mirids attacks cause substantial losses in cacao production. Black pod disease darkens the affected areas of cacao pods, while the cacao mirids (*Sahlbergella singularis*) is a major pest in West African plantations. Together, these threats significantly reduce crop yield and shorten the lifespan of the plants. This study evaluates production losses caused by the combined effects of Miridae infestation and black pod disease. We formulate and analyze a mathematical model incorporating spores, pods, and Miridae populations, governed by a system of ordinary differential equations. Theoretical analyses include equilibrium computations and threshold conditions for optimal plantation productivity. The analytical findings are validated through numerical simulations. We also examine the effects of three control strategies, Phytosanitary measures, Miridae control, and their combined application on production optimization. These strategies are modeled using impulsive differential equation systems. Our key quantitative findings show that black pod disease alone causes approximately 88.94% production loss, Miridae alone cause 34.21% loss, and co-infection leads to near-total losses exceeding 90%.

**Keywords:** cacao production; Miridae pests; black pod disease; mathematical modeling; vector–host dynamics; impulsive differential equations; pest management

## 1. Introduction

Cocoa production plays a vital role in multiple industries because of its versatility. It is most renowned for its contribution to chocolate manufacturing, where cocoa beans are processed into cocoa solids and cocoa butter, essential ingredients for dark, milk, and white chocolate. Beyond confectionery, cocoa is widely used in baked goods, beverages, dietary supplements, and cosmetics, highlighting its broad economic and cultural significance. Globally, approximately 5–6 million farmers contribute 90–95% of cacao production, predominantly through smallholder farms inWest and Central Africa. Key producers include Ivory Coast, Ghana, Nigeria, Cameroon, and Togo, with Ivory Coast being the largest global producer [1, 2]. In Cameroon alone, 400,000–600,000 families are involved in cocoa cultivation, with about 95% operating small farms of 2.5–5 hectares. Cocoa is a key cash crop that supports livelihoods and local economies.

Cacao production faces significant challenges from pests and diseases. Black pod rot, caused by *Phytophthora* species such as *P. palmivora* and *P. megakarya*, can reduce yields by 80–90% in poorly managed plantations [3,4]. In Cameroon, *P. megakarya* has become the predominant agent of black pod rot. Concurrently, Miridae pests, particularly Sahlbergella singularis, are widespread and can cause 30–40% losses in potential production [5]. Another notable pest is *Distantiella theobroma*. Understanding these threats and their interactions is essential for designing effective management strategies. While several mathematical models have examined Miridae populations'dynamics [6, 7, 10] and black pod disease spread [8, 9] separately, few models have examined the combined impact of both threats or explore the co–infection dynamics. The present work extends previous studies by explicitly coupling pest and pathogen dynamics, thereby providing a unified framework that captures the synergistic effects of co–infection on cacao production losses.

This paper addresses these gaps by formulating a coupled model that integrates Miridae pests, black pod rot, and cacao pod development. The model accounts for pod stages, spore classes, and Miridae life stages (eggs and adults). Each sub–model is analyzed to determine the equilibria, stability, and production losses. The complete system allows the identification of coexistence thresholds and conditions under which Miridae infestations can exacerbate disease, and vice versa. The paper is organized as follows: Section 2 presents the mathematical model for interactions among Miridae, black pod rot, and pod development; Section 3 provides mathematical analysis, including sub-model studies and reciprocal impacts, and Section 4 concludes with key findings and implications for sustainable cacao management.

## 2. Model construction

### *2.1. Biological background for modeling purposes*

*Phytophthora megakarya* is the causative agent of black pod rot, the most damaging disease affecting cocoa production. Its life cycle includes four stages: the mycelial stage, sporangia, zoospores, and chlamydospores (see Figure 1(a) for details). Sporangia serve as the primary infection source and require free water to release zoospores. These zoospores spread the pathogen either directly through rainfall and infected debris or indirectly via insects and human activities, particularly under favorable rainy conditions.

The most harmful pest affecting cocoa crops is *Sahlbergella singularis*, a member of the Miridae

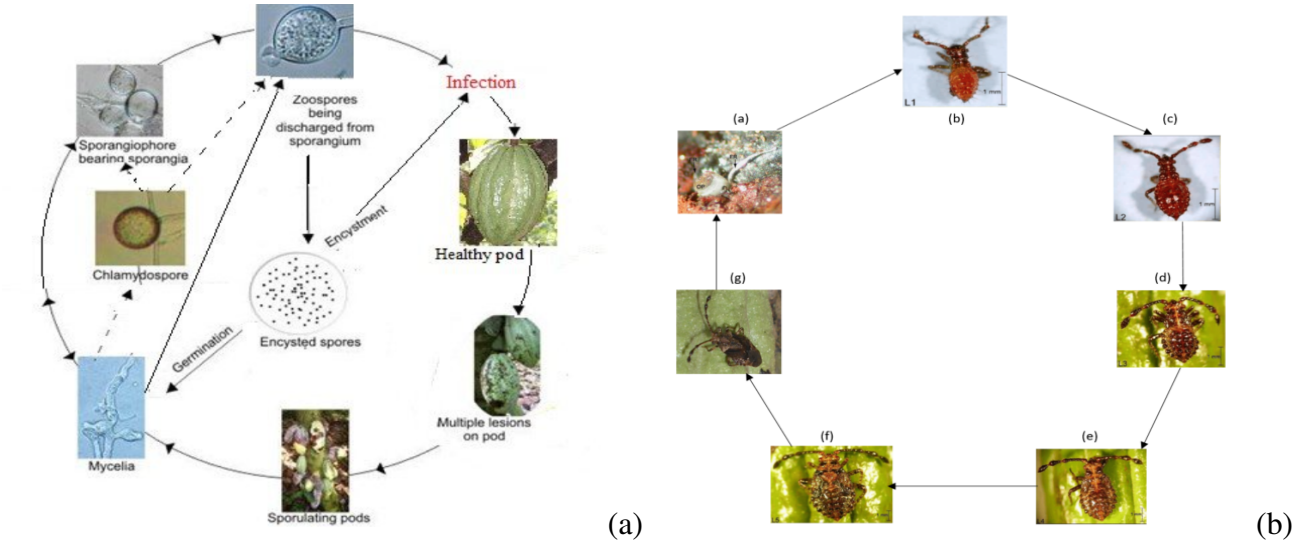


**Figure 1.** (a) Life cycle of *Phytophthora megakarya* on cacao, highlighting the main spore types and infective propagules [8]. (b) Life cycle of *Sahlbergella singularis*: (a) Eggs, (b) Nymphs $L_1$, (c) Nymphs $L_2$, (d) Nymphs $L_3$, (e) Nymphs $L_4$, (f) Nymphs $L_5$ and (g) adults.

family. Its life cycle comprises three key stages: Eggs, nymphs, and adults (see Figure 1(b) for details). Adult mirids feed on cocoa pods and lay eggs within them, causing substantial damage. Previous studies have used mathematical models to estimate the extent of damage caused by these pests [10].

The growth cycle of cacao pods can typically be divided into three subphases. The first phase, known as the ”cherelle” stage, is when fruits are highly susceptible to physiological deterioration, commonly referred to as ”cherelle wilt” [14]. The final phase corresponds to fully ripe pods.

### *2.2. The model framework*

The formulation of the model builds upon the life cycles of cacao pods and the organisms that affect them. The primary disease considered is black pod rot, caused by species of Phytophthora, notably *Phytophthora megakarya*, which is responsible for severe yield losses and plant deterioration.

Cacao growth and *Sahlbergella singularis* (Miridae) development proceed through three main stages: Cherelles, young pods, and ripe pods for cacao, and eggs, nymphs, and adults for Miridae.Adult insects feed on pods and lay eggs inside them, causing substantial physical and physiological damage to both pods and trees.

While the effects of Miridae damage have previously been modeled mathematically [10], this study investigates the combined impact of Miridae infestations and black pod rot on cacao production. The model includes three interacting populations: Miridae, cacao pods, and fungal spores. Cacao pods are divided into two epidemiological classes: Susceptible and infected. Infected pods are grouped into three categories: Pods damaged by Miridae ($I_m$), pods infected by black pod rot ($I_p$), and pods affected by both agents (co–infected pods, $I_{mp}$).

We also consider two classes within the Miridae population: Eggs ($E$) laid by adult females, and Miridae ($M$), representing all biting life stages (nymphs and adults). In addition, a single class describes the spore population ($P$). The overall system is illustrated in Figure 2.

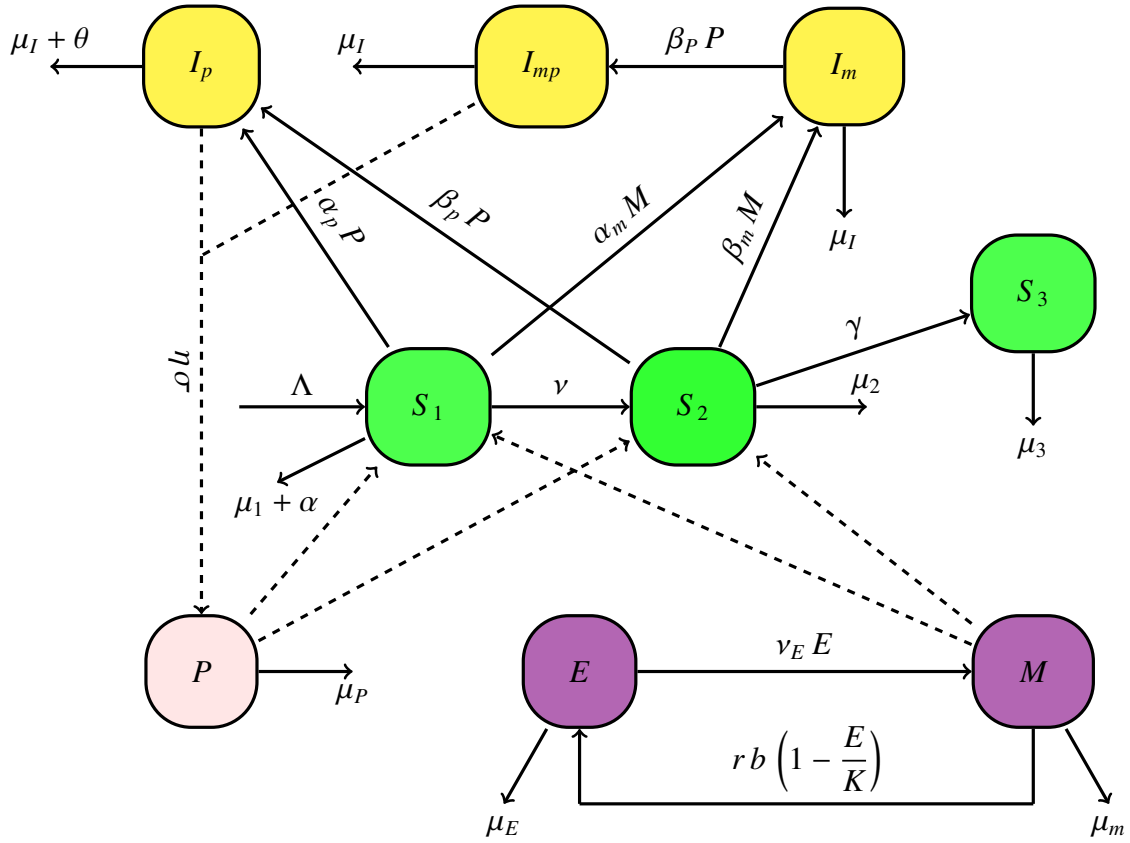


**Figure 2.** Flowchart of the model for cacao infection dynamics, illustrating the interactions among susceptible pods ($S_1, S_2$), ripe pods ($S_3$), spores ($P$), and Miridae vectors ($M$) in disease transmission and the progression of affected pods ($I_m, I_p, I_{mp}$).

In the cherelle stage, pods enter the system at a constant rate $\Lambda$. The parameters $\mu_1$, $\alpha$, and $\nu$ represent the natural death rate, the additional death rate due to cherelle wilt, and the maturation rate, respectively. Wilt is a natural physiological process that regulates pod density on the tree. For the young pod stage, $\gamma$ denotes the maturation rate to ripe pods, and $\mu_2$ the natural death rate of young pods.

Pods infected by black pod rot ($I_p$) result from contact between susceptible pods and spores, either from environmental sources or directly from other infected pods. Susceptible pods (cherelles and young pods) are infected following the principle of mass action, with the rates $\alpha_p P$ for cherelles and $\beta_p P$ for young pods. Co–infected pods ($I_{mp}$) are those first damaged by Miridae bites and subsequently contaminated by spores, also at the rate $\beta_p P$. Because Miridae prefer to feed on healthy pods, we assume that pods already infected by black pod rot cannot be further bitten. The parameters $\alpha_p$ and $\beta_p$ thus represent the maximal infection rates for cherelles and young pods, respectively. The parameters $\theta$ and $\mu_I$ represent the phytosanitary removal rate of infected pods and their average death rate.

Pods damaged by Miridae ($I_m$) emerge when susceptible pods (cherelles or young pods) are bitten by Miridae, at the rates $\alpha_m M$ and $\beta_m M$, respectively. Here, $\alpha_m$ (for cherelles) and $\beta_m$ (for young pods) denote the probabilities that a bite leads to damage. Continued feeding and oviposition further damage affected pods, captured by the loss term $-dI_m M$, which represents additional mortality due to intensive

Miridae activity.

The Miridae population includes both eggs ($E$) and biting individuals ($M$). Egg production is limited by a carrying capacity $K$, reflecting resource constraints. The parameter $r$ represents the sex ratio, $1/\nu_E$ is the time required for eggs to develop into adults, $\mu_E$ is the egg mortality rate, $d$ is the feeding and oviposition efficiency, $e$ is the biomass conversion rate, and $\mu_m$ is the adult mortality rate.

Spores are produced by infected pods ($I_p$ and $I_{mp}$), which release them into the environment and thereby perpetuate infection. The rate of spore production is $\sigma$, $\eta$ represents the rate of spore release, and $\mu_p$ is the rate of spore inactivation due to parasitism, senescence, or natural decay. The term $\beta_p I_m P$ appears in the equations for $I_{mp}$ (representing contamination of Miridae–damaged pods by spores) and correctly does not appear in the $I_p$ equation, as pods already infected by black pod rot cannot be subsequently damaged by Miridae under our unidirectional assumption.

Co-infection is assumed to be unidirectional: Pods damaged by Miridae can be subsequently infected by black pod rot, but not vice versa. This simplification is justified by field observations that Miridae preferentially attack healthy pods rather than those already showing signs of fungal infection, though direct experimental evidence remains limited [11–13]. Future field studies should test this assumption explicitly.

Parameter values for spore and pod dynamics were derived from published sources, while parameters associated with Miridae–induced damage were based on expert knowledge and biological reasoning. The model considers a spatial scale of 1 hectare, typically containing about 1200 cacao trees. Following the empirical observations in [28], each tree produces approximately 12 cherelles per day, corresponding to about 14,400 new cherelles daily per hectare. The transmission rates $\alpha_m$, $\beta_m$, $\alpha_p$, and $\beta_p$ are per–capita rates scaled to this spatial unit of 1 hectare with 1200 trees, assuming homogeneous mixing within the plantation.

We assume a well–mixed population within this spatial scale, ignoring fine–scale stochastic fluctuations and spatial heterogeneity. This simplification allows the analysis of system–level trends, though it limits the ability to capture localized outbreaks or inter-plantation spread. The model does not include direct interaction terms between the two diseases, but represents co-infection as a one–way process from Miridae–induced to black pod–induced infection.

Finally, only young pods are considered harvestable; once a pod becomes infected, it is excluded from harvest. The complete model therefore integrates the biological processes governing pod development, Miridae dynamics, and spore transmission into a unified mathematical framework.

The temporal evolution of the system is described by a set of nonlinear ordinary differential equations (Eq. (2.1)), which capture the interactions among pods, spores, and Miridae populations over time. These equations form the basis for subsequent theoretical and numerical analyses, including the

study of equilibrium points, threshold conditions, and control strategies.

$$\begin{cases} \dot{S}_1 &= \Lambda - (\nu + \mu_1 + \alpha) S_1 - \alpha_m S_1 M - \alpha_p S_1 P, \\ \dot{S}_2 &= \nu S_1 - (\gamma + \mu_2) S_2 - \beta_m S_2 M - \beta_p S_2 P, \\ \dot{I}_m &= \alpha_m S_1 M + \beta_m S_2 M - \mu_I I_m - \beta_p I_m P - d I_m M, \\ \dot{I}_{mp} &= \beta_p I_m P - \mu_I I_{mp}, \\ \dot{I}_p &= \alpha_p S_1 P + \beta_p S_2 P - (\mu_I + \theta) I_p, \\ \dot{S}_3 &= \gamma S_2 - \mu_3 S_3, \\ \dot{P} &= \eta \sigma (I_p + I_{mp}) - \mu_p P, \\ \dot{E} &= r b M \left(1 - \frac{E}{K}\right) - (\nu_E + \mu_E) E, \\ \dot{M} &= \nu_E E + e d I_m M - \mu_m M \quad , \end{cases} \tag{2.1}$$

with positive initial conditions given by

$$\begin{cases} S_1(0) = S_1^0, \quad S_2(0) = S_2^0, \quad I_m(0) = I_m^0, \quad S_3(0) = S_3^0, \\ I_p(0) = I_p^0, \quad I_{mp}(0) = I_{mp}^0, \quad P(0) = P^0, \quad E(0) = E^0, \quad M(0) = M^0. \end{cases} \tag{2.2}$$

Tables 1 and 2 provide a comprehensive list of all variables and parameters of System (2.1), along with their respective values and references.

**Table 1.** Variables of System (2.1).

| Symbol | Biological meaning |
|---|---|
| $S_1$ | Cherelle pods |
| $S_2$ | Young pods |
| $I_m$ | Pods damaged by Miridae attacks |
| $I_p$ | Pods infected by black pod rot |
| $I_{mp}$ | Co-infected pods (Miridae damage and black pod rot) |
| $S_3$ | Ripe pods |
| $P$ | Spore population in the plot |
| $E$ | Egg population of Miridae in the plot |
| $M$ | Miridae population (nymphs and adults) in the plot |

**Table 2.** Parameter description of System (2.1).

| Parameter | Description | Values | Unit | References |
|---|---|---|---|---|
| $\Lambda$ | Cherelle recruitment rate | 14,400 | Cherelles·days$^{-1}$ | Assumed |
| $\nu$ | Progression rate from cherelle to young pod | 0.05 | days$^{-1}$ | [16] |
| $\gamma$ | Progression rate from young pod to ripe pod | 0.027 | days$^{-1}$ | [8] |
| $\alpha$ | Additional death rate due to wilt | 0.1 | days$^{-1}$ | [15] |
| $\alpha_m$ | Damage rate of cherelle stage due to Miridae attacks | 0.00002 | days$^{-1}$·Miridae$^{-1}$ | Assumed |
| $\beta_m$ | Damage rate of young pods due to Miridae attacks | 0.00001 | days$^{-1}$·Miridae$^{-1}$ | Assumed |
| $\alpha_p$ | Infection rate of cherelle stage due to black pod rot | 0.00001 | days$^{-1}$·Spores$^{-1}$ | Assumed |
| $\beta_p$ | Infection rate of the young pods stage due to black pod rot | 0.0002 | days$^{-1}$·Spores$^{-1}$ | Assumed |
| $\mu_1$ | Natural death rate of cherelles | 0.05 | days$^{-1}$ | [16] |
| $\mu_2$ | Natural death rate of young pods | 0.00469 | days$^{-1}$ | [16] |
| $\mu_3$ | Natural death rate of ripe pods | 0.0469 | days$^{-1}$ | Assumed |
| $\mu_I$ | Natural death rate of infected pods | 0.05 | days$^{-1}$ | Assumed |
| $\theta$ | Rate of phytosanitary pod removal | 0.3 | days$^{-1}$ | [22] |
| $e$ | Biomass conversion rate | 0.000001 | dimensionless | Assumed |
| $d$ | Feeding and egg-laying efficiency rate | 0.000001 | days$^{-1}$ | Assumed |
| $\eta$ | Releasing speed of spore | 0.04 | days$^{-1}$ | Assumed |
| $\sigma$ | Production rate of spores by infected pods | 10 | days$^{-1}$ | Assumed |
| $\mu_p$ | Natural death rate of spores | 0.02 | days$^{-1}$ | [8] |
| $r$ | Sex ratio of Miridae population | 0.58 | dimensionless | [17] |
| $b$ | Mean number of eggs laid by a mature female mirid | 3.28 | Miridae$^{-1}$·days$^{-1}$ | [6] |
| $1/\nu_E$ | Time for an egg to become an adult mirid | 15 | days | [6] |
| $\mu_E$ | Mortality of Miridae eggs | 0.001 | days$^{-1}$ | [6] |
| $K$ | Carrying capacity for eggs | 5000 | dimensionless | Assumed |
| $\mu_m$ | Mortality rate of adult Miridae | 0.07 | days$^{-1}$ | [6] |

## 3. Model analysis

In this section, we perform a qualitative analysis of Model (2.1) to gain a deeper understanding of the dynamics governing the evolution of Miridae and black pod disease. This analysis includes proving the positivity and boundedness of each population, establishing the existence and stability of steady–state solutions, calculating threshold quantities, and exploring potential bifurcation phenomena. We start by analyzing the spores–pods and Miridae–pods submodels, followed by a presentation of the generalized results for the co-infection model (2.1).

### *3.1. Basic properties of Model (2.1)*

Model (2.1) describes the interactions between the pods, spores, and Miridae populations. It can be shown that the state variables associated with the model are non–negative for all $t \geq 0$, and that the solutions of Model (2.1) with positive initial conditions remain positive for all $t \geq 0$. Furthermore, we assume that the associated parameters are non–negative for all $t \geq 0$, and we will demonstrate that all feasible solutions are uniformly bounded within a proper subset $\Omega$.

**Lemma 1.** *For any non-negative initial conditions, all solutions of Model (2.1) remain non-negative for all $t \geq 0$.*

System (2.1) can be rewritten as

$$\begin{cases} \dfrac{dX}{dt} = A(X)\,X + F, \\ X(0) = X_0 \geq 0, \end{cases} \tag{3.1}$$

where $X = (S_1,\, S_2,\, I_m,\, I_{mp},\, I_p,\, S_3,\, P,\, E,\, M)^T$,

$$A(X) = \begin{pmatrix} -a_1 & 0 & 0 & 0 & 0 & 0 & 0 & 0 & 0 \\ \nu & -a_2 & 0 & 0 & 0 & 0 & 0 & 0 & 0 \\ \alpha_m M & \beta_m M & -a_3 & 0 & 0 & 0 & 0 & 0 & 0 \\ 0 & 0 & \beta_p P & -\mu_I & 0 & 0 & 0 & 0 & 0 \\ \alpha_p P & \beta_p P & 0 & 0 & -(\mu_I + \theta) & 0 & 0 & 0 & 0 \\ 0 & \gamma & 0 & 0 & 0 & -\mu_3 & 0 & 0 & 0 \\ 0 & 0 & 0 & \eta\sigma & \eta\sigma & 0 & -\mu_p & 0 & 0 \\ 0 & 0 & 0 & 0 & 0 & 0 & 0 & -(\nu_E + \mu_E) & r\,b\left(1 - \dfrac{E}{K}\right) \\ 0 & 0 & e\,d\,I_m & 0 & 0 & 0 & 0 & \nu_E & -\mu_m \end{pmatrix},$$

and

$$F = (\Lambda,\, 0,\, 0,\, 0,\, 0,\, 0,\, 0,\, 0,\, 0)^T$$

with

$$a_1 = \nu + \mu_1 + \alpha + \alpha_m M + \alpha_p P, \quad a_2 = \gamma + \mu_2 + \beta_m M + \beta_p P, \quad a_3 = \mu_I + \beta_p P + d M \quad .$$

The matrix $\mathcal{A}(X)$ is a Metzler matrix, and $F \geq 0$. Therefore, System (2.1) is positively invariant in $\mathbb{R}^9_+$ [24]. This implies that any trajectory of the system, starting from an initial state in the positive orthant $\mathbb{R}^9_+$, will remain in $\mathbb{R}^9_+$ for all $t \geq 0$.

**Theorem 1.** *The domain*

$$\begin{aligned}\Omega =\{&(S_1,\, S_2,\, I_m,\, I_{mp},\, I_p,\, S_3,\, P,\, E,\, M) \in \mathbb{R}^9_+\ S_1 \leq S_1^{\max},\ S_2 \leq S_2^{\max},\ I_m \leq I_m^{\max},\ I_{mp} \leq I_{mp}^{\max},\\ &I_p \leq I_p^{\max},\ S_3 \leq S_3^{\max},\ P \leq P^{\max},\ E \leq E^{\max},\ M \leq M^{\max}.\}\end{aligned}$$

*where*

$$S_1^{\max} = \frac{\Lambda}{\nu + \mu_1 + \alpha}, \quad S_2^{\max} = \frac{\nu S_1^{\max}}{\gamma + \mu_2}, \quad I_m^{\max} = \frac{\alpha_m S_1^{\max} M^{\max} + \beta_m S_2^{\max} M^{\max}}{\mu_I},$$

$$I_{mp}^{\max} = \frac{\beta_p I_m^{\max} P^{\max}}{\mu_I}, \quad I_p^{\max} = \frac{\alpha_p S_1^{\max} + \beta_p S_2^{\max}}{\mu_I + \theta},$$

$$S_3^{\max} = \frac{\gamma S_2^{\max}}{\mu_3}, \quad P^{\max} = \frac{\eta \sigma I_p^{\max}}{\mu_p}, \quad E^{\max} = K \quad \textit{and} \quad M^{\max} = \frac{\nu_E K}{\mu_m - e\, d\, I_m^{\max}}$$

*is positively invariant for Model (2.1).*

**Remark 1.** *The domain $\Omega$ is realistic if $\mu_m > e\, d\, I_m^{\max}$, which ensures non–negativity. Using the baseline parameter values from Table 2, we verify that $\mu_m = 0.07$ and $edI_m^{\max} \approx 0.000001 \times 0.000001 \times I_m^{\max}$, which is satisfied for realistic $I_m^{\max}$ values. This condition holds under typical plantation conditions but could be violated if Miridae-induced mortality becomes extremely high.*

**Proof**: From the first equation of System (2.1), we have

$$\dot{S}_1(t) = \Lambda - (\nu + \mu_1 + \alpha)\, S_1(t) - \alpha_p\, S_1(t)\, P(t) - \alpha_m\, S_1(t)\, M(t) \leq \Lambda - (\nu + \mu_1 + \alpha)\, S_1 \quad .$$

Solving this inequality leads to

$$S_1(t) \leq S_1^{\max} + (S_1(0) - S_1^{\max}) e^{-(\nu+\mu_1+\alpha)t} \quad .$$

Thus, if $S_1(0) \leq S_1^{\max}$, we can deduce that

$$0 \leq S_1(t) \leq S_1^{\max} \quad \text{for all } t \geq 0 \quad .$$

Similarly, one can prove that $S_2(t) \leq S_2^{\max}$ and $S_3(t) \leq S_3^{\max}$ for all $t \geq 0$.
From the eighth equation of System (2.1), we have

$$\dot{E}(t) = r\, b\, M(t) \left(1 - \frac{E(t)}{K}\right) - (\nu_E + \mu_E)\, E(t) \quad .$$

Assume that exists $\varepsilon > 0$ such that

$$t_1 \leq t_1 + \varepsilon < T \quad \text{and} \quad E(t_1 + \varepsilon) > K \quad .$$

Now define

$$t_1^* = \inf\{t \geq t_1 : E(t) \geq K\}.$$

It follows that

$$E(t_1^*) = K \quad .$$

Thus we have

$$E(t) = E(t_1^*) + \dot{E}(t_1^*)(t - t_1^*) + o(t - t_1^*) \quad \text{and} \quad \dot{E}(t_1^*) = -(\nu_E + \mu_E)E(t_1^*) < 0 \quad .$$

So, exists $\varepsilon_1 > 0$ such that

$$t_1^* \leq t < t_1^* + \varepsilon_1 \quad \text{and} \quad E(t_1^*) < K \quad .$$

This leads to a contradiction because $t_1^* = \inf\{t \geq t_1,\, E(t) \geq K\}$. Consequently, $E(t) \leq K$ for all $t \geq t_0$. By integrating the equations for $M$, $I_m$, $I_{mp}$, $I_p$, and $P$ separately in System (2.1) and applying Gronwall's lemma, we can show that

$$M(t) \leq M^{\max}, \quad I_m(t) \leq I_m^{\max}, \quad I_{mp}(t) \leq I_{mp}^{\max}, \quad I_p(t) \leq I_p^{\max}, \quad \text{and} \quad P(t) \leq P^{\max} \text{ for all } t \geq 0.$$

This concludes the proof. □

3.1.1. Model reduction

The $S_3$ (ripe pods) compartment is decoupled from the infection dynamics because ripe pods are no longer susceptible to infection and do not contribute to spore production or Miridae population growth. Therefore, we can simplify our analysis by focusing on the compartments that are critical for understanding the dynamics of the system. Therefore, we deduce that our system is governed by the following system of ordinary differential equations:

$$\begin{cases} \dot{S}_1 &= \Lambda - (\nu + \mu_1 + \alpha)\, S_1 - \alpha_m\, S_1\, M - \alpha_p\, S_1\, P, \\ \dot{S}_2 &= \nu\, S_1 - (\gamma + \mu_2)\, S_2 - \beta_m\, S_2\, M - \beta_p\, S_2\, P, \\ \dot{I}_m &= \alpha_m\, S_1\, M + \beta_m\, S_2\, M - \mu_I\, I_m - \beta_p\, I_m\, P - d\, I_m\, M, \\ \dot{I}_{mp} &= \beta_p\, I_m\, P - \mu_I\, I_{mp}, \\ \dot{I}_p &= \alpha_p\, S_1\, P + \beta_p\, S_2\, P - (\mu_I + \theta)\, I_p, \\ \dot{P} &= \eta\, \sigma\, (I_p + I_{mp}) - \mu_p\, P, \\ \dot{E} &= r\, b\, M \left(1 - \dfrac{E}{K}\right) - (\nu_E + \mu_E)\, E, \\ \dot{M} &= \nu_E\, E + e\, d\, I_m\, M - \mu_M\, M \quad . \end{cases} \tag{3.2}$$

This system captures the essential dynamics of disease transmission without the additional complexity introduced by the $S_3$ compartment.

For a better understanding of the dynamics of co-infection using the proposed reduced model (3.2), we first compute the equilibrium points of the model and then examine the dynamics around those stationary points. The detailed analysis will focus on the behavior of each submodel solutions near the equilibrium points for spores–pods model, Miridae–pods model, and the coinfection model.

### 3.1.2. Sensitivity analysis of model (2.1)

We performed the sensitivity analysis using a partial rank correlation coefficient (PRCC) in order to evaluate the sensitivity of the model output to variations in key parameters. The result is given in Figure 3. This result indicates that the recruitment rate ($\Lambda$) has the strongest positive influence ($PRCC \approx 0.7$), implying that increased inflow into the susceptible population substantially enhances disease transmission. Similarly, the pathogen production parameters ($\eta$) and ($\sigma$) exhibit notable positive sensitivity, highlighting their role in amplifying environmental pathogen. Transmission-related parameters, including ($\alpha_m$), ($\alpha_p$), ($\beta_m$), and ($\beta_p$), show moderate positive effects, confirming their contribution to infection spread. In contrast, natural mortality parameters ($\mu_1$, $\mu_2$, $\mu_3$) display relatively weak negative correlations, suggesting a limited influence on overall dynamics.

On the other hand, several parameters demonstrate strong negative influence the model. The recovery or removal rate ($\theta$) emerges as the most influential mitigating factor ($PRCC \approx -0.6$), indicating that increasing recovery significantly reduces disease prevalence. The pathogen decay rate ($\mu_p$) also shows a negative effect, emphasizing the importance of reducing environmental pathogen persistence. Additionally, the infected mortality rate ($\mu_I$) contributes negatively, with a moderate magnitude. Overall, the PRCC analysis reveals that disease dynamics are primarily driven by recruitment and pathogen production processes, while recovery and pathogen decay play critical roles in controlling the spread of infection. These findings provide valuable insights for designing effective intervention strategies.

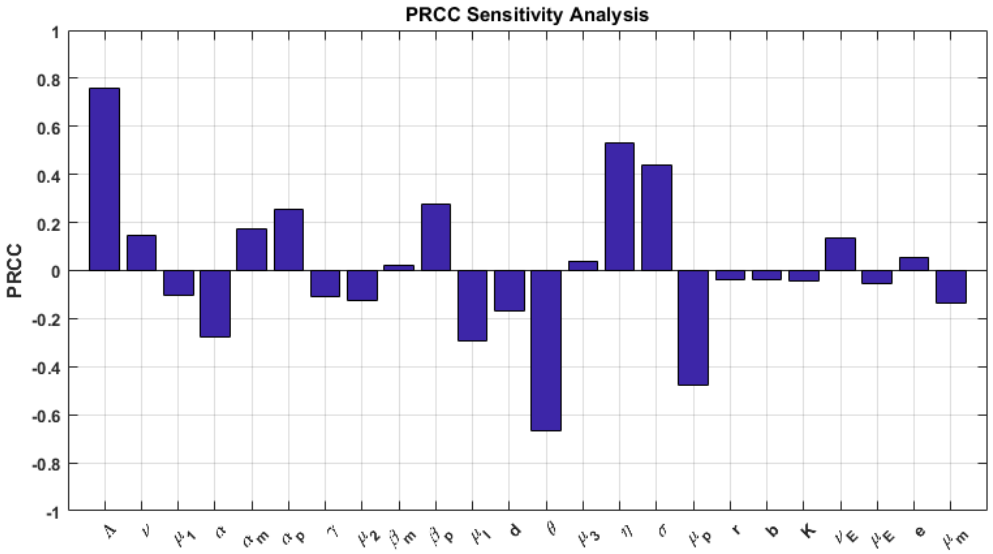


**Figure 3.** PRCC sensitivity analysis of Model (2.1).

### 3.2. Spores–pods model

Here, we present the theoretical results of the spores–pods model. By setting $I_m = M = 0$ in System (3.2), the spores–pods model is governed by the following system of ordinary differential equations:

$$\begin{cases} \dot{S}_1 &= \Lambda - (\nu + \mu_1 + \alpha) S_1 - \alpha_p S_1 P \quad , \\ \dot{S}_2 &= \nu S_1 - (\gamma + \mu_2) S_2 - \beta_p S_2 P \quad , \\ \dot{I}_p &= \alpha_p S_1 P + \beta_p S_2 P - (\mu_I + \theta) I_p \quad , \\ \dot{P} &= \eta \sigma I_p - \mu_p P \quad , \end{cases} \tag{3.3}$$

with initial conditions $S_1(0) > 0$, $S_2(0) \geq 0$, $I_p(0) \geq 0$, and $P(0) > 0$ .

#### 3.2.1. Stability of disease-free equilibrium (DFE) of the spores-pods sub-model (3.3)

The DFE of the spores–pods model (3.3) is obtained by setting all the equations in System (3.3) to zero. Since there are no infections at the DFE, the equilibrium of the spores–pods sub–model (3.3) is given by

$$\mathcal{Q}^0 = (S_1^0, S_2^0, 0, 0) = \left( \frac{\Lambda}{\nu + \mu_1 + \alpha}, \frac{\Lambda \nu}{(\gamma + \mu_2)(\nu + \mu_1 + \alpha)}, 0, 0 \right) \quad . \tag{3.4}$$

Using the next-generation approach developed by Van den Driessche and Watmough [18], we compute the basic reproduction number $\mathcal{R}$, which, in this case, represents the number of new infections produced by an infectious pod when introduced into a population of healthy pods of any maturity stage. To do this, we rewrite System (3.3) as

$$\dot{x} = f(x) = \mathcal{F}(x) - \mathcal{V}(x), \tag{3.5}$$

where $x = (I_p, P)$, $\mathcal{F}$ is the rate of new infections in each class, and $\mathcal{V}(x)$ represents the transfer rate of individuals into and out of each compartment. Hence, we have

$$\mathcal{F} = \begin{pmatrix} \alpha_p S_1 P + \beta_p S_2 P \\ \\ \eta \sigma I_p \end{pmatrix} \quad \text{and} \quad \mathcal{V} = \begin{pmatrix} (\mu_I + \theta) I_p \\ \\ \mu_p P \end{pmatrix}.$$

The Jacobian matrices of $\mathcal{F}$ and $\mathcal{V}$ evaluated at the DFE $\mathcal{Q}^0$ are

$$F = \begin{pmatrix} 0 & \alpha_p S_1^0 + \beta_p S_2^0 \\ \\ 0 & 0 \end{pmatrix} \quad \text{and} \quad V = \begin{pmatrix} \mu_I + \theta & 0 \\ \\ 0 & \mu_p \end{pmatrix}.$$

The basic reproduction number, $\mathcal{R}$, is defined as the spectral radius (dominant eigenvalue) of the next-generation matrix $FV^{-1}$

$$\mathcal{R} = \left( \frac{\eta \sigma (\alpha_p S_1^0 + \beta_p S_2^0)}{\mu_p (\mu_I + \theta)} \right)^{1/2} = \left( \frac{\eta \sigma \Lambda (\beta_p \nu + \alpha_p (\gamma + \mu_2))}{\mu_p (\mu_I + \theta)(\mu_2 + \gamma)(\nu + \mu_1 + \alpha)} \right)^{1/2} \quad .$$

**Lemma 2.** *The expression for $\mathcal{R}$ quantifies the number of secondary infections caused by an infectious pod in a fully susceptible population, considering both mature and immature pods.*

We have the following result on the global asymptotic stability of the DFE $\mathcal{Q}^0$ of System (3.3).

**Theorem 2.** *The DFE $\mathcal{Q}^0$ of the System (3.3) is globally asymptotically stable in $\Omega$ when $\mathcal{R} \leq 1$ and unstable when $\mathcal{R} > 1$. This implies that there will be no infection in the plot when $\mathcal{R} \leq 1$.*

**Proof**: Consider the following Lyapunov function candidate:

$$V(X) = \eta\,\sigma\, I_P + (\mu_I + \theta)\, P, \tag{3.6}$$

where $X = (S_1, S_2, I_P, P)^T$. Its time derivative satisfies

$$\begin{aligned} \dot{V} &= \eta\,\sigma\,\dot{I}_p + (\mu_I + \theta)\,\dot{P} \quad , \\ &= \eta\,\sigma\,\left[(\alpha_p\, S_1 + \beta_p\, S_2)\, P - (\mu_I + \theta)\, I_p\right] + (\mu_I + \theta)(\eta\,\sigma\, I_p - \mu_p\, P) \quad , \\ &= \eta\,\sigma\,(\alpha_p\, S_1 + \beta_p\, S_2)P - (\mu_I + \theta)\mu_p P \quad . \end{aligned} \tag{3.7}$$

Since $S_1(t) \leq S_1^0$ and $S_2(t) \leq S_2^0$ for all $t \geq 0$, Equation (3.7) becomes

$$\begin{aligned} \dot{V} &\leq \eta\,\sigma\,(\alpha_p\, S_1^0 + \beta_p\, S_2^0)P - (\mu_I + \theta)\mu_p P \\ &= \mu_p(\mu_I + \theta)P\left[\frac{\eta\,\sigma\,(\alpha_p\, S_1^0 + \beta_p\, S_2^0)}{\mu_p(\mu_I + \theta)} - 1\right] \\ &\leq \mu_p(\mu_I + \theta)P\left(\mathcal{R}^2 - 1\right). \end{aligned} \tag{3.8}$$

Hence, $\dot{V} \leq 0$ whenever $\mathcal{R} \leq 1$. Furthermore,

$$\dot{V} = 0 \Longleftrightarrow P = 0 \quad \text{or} \quad S_1 = S_1^0, \quad S_2 = S_2^0 \quad \text{and} \quad \mathcal{R} = 1 \quad .$$

Thus, the largest invariant set $\mathcal{H}$ contained in $\{X \in \Omega,\ \dot{V}(X) = 0\}$ is the singleton $\mathcal{Q}^0$. By LaSalle's invariance principle [23], $\mathcal{Q}^0$ is globally asymptotically stable in $\Omega$. This completes the proof. □

**Remark 2.** *When $\mathcal{R} \leq 1$, optimal production in the plot is achieved and given by*

$$S_3 = \frac{\Lambda\,\nu}{\mu_3\,(\gamma + \mu_2)\,(\nu + \mu_1 + \alpha)}.$$

It is important to determine the parameters that impact the basic reproduction number $\mathcal{R}$ and the production $S_3$. To do this, we perform sensitivity analysis of $\mathcal{R}$ and $S_3$. The parameter values used for the sensitivity analysis are provided in Table 2.

Figure 4 presents the sensitivity analysis of the basic reproduction number $\mathcal{R}$ and the optimal production $S_3$. The results indicate that $\mathcal{R}$ is significantly impacted by parameters such as $\eta$, $\sigma$, and $\Lambda$, which have a positive effect, and by $\mu_p$ and $\mu_I$, which have a negative effect. Similarly, the production $S_3$ is primarily influenced by $\Lambda$ and $\nu$, both contributing positively, while $\mu_3$ and $\gamma$ negatively affect it.

Now, we will illustrate this theory through numerical simulations. We consider a density of $1,200$ cocoa plants per hectare, which aligns with the recommended spacing of 2 to 3 meters between cocoa tree rows. This density reflects the average cultivation practices in Africa [25]. The initial conditions

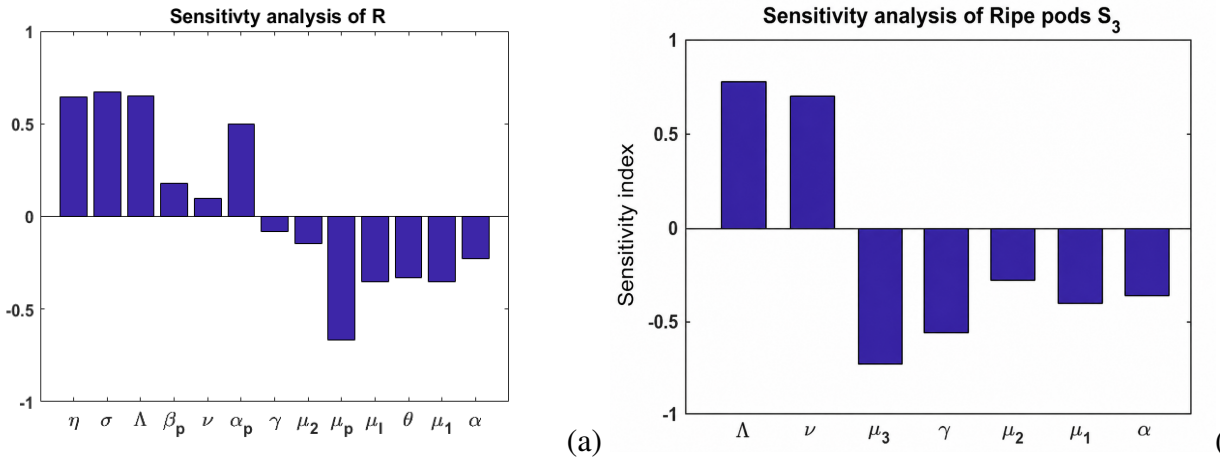


**Figure 4.** Sensitivity analysis of the basic reproduction number $\mathcal{R}$ and the optimal production of ripe pods $S_3$.

are $S_1(0) = 1000$, $S_2(0) = 500$, $S_3(0) = I_p(0) = 0$, and $P(0) = 100$, chosen arbitrarily.
Figure 5 (on Page 2669) presents the trajectories of System (3.3) using various initial conditions. Blue, red, and green colours represent respectively the phase plane (infectious pods, cherelle, and young pods), the ripe pods and spores'evolution. It is evident that these trajectories converge to the DFE $Q^0$, as shown in Theorem 2. This indicates that the disease disappears within the cocoa plot, resulting in optimal production.

3.2.2. The endemic equilibrium of sub–model (3.3)

Let $(\overline{S}_1, \overline{S}_2, \overline{I}_p, \overline{P})$ be the endemic equilibrium of Eq. (3.3). The endemic equilibrium is obtained by setting System (3.3) equal to zero, leading to the following polynomial equation:

$$a_2 P^2 + a_1 P + a_0 = 0 \tag{3.9}$$

The coefficients are now correctly labeled $a_2$, $a_1$, $a_0$ (not $a_3$), where

$$\begin{aligned} a_2 &= \alpha_p \beta_p \mu_p (\mu_I + \theta), \\ a_1 &= \mu_p (\mu_I + \theta)(\alpha_p (\gamma + \mu_2) + \beta_p (\nu + \mu_1 + \alpha)) - \eta \sigma \Lambda \alpha_p \beta_p, \\ a_0 &= \mu_p (\mu_I + \theta)(\nu + \mu_1 + \alpha)(\gamma + \mu_2)(1 - \mathcal{R}^2). \end{aligned}$$

Explicitly, the endemic equilibrium is given by:

$$\overline{S}_1 = \frac{\Lambda}{\nu + \mu_1 + \alpha + \alpha_p \overline{P}}, \quad \overline{S}_2 = \frac{\nu \overline{S}_1}{\gamma + \mu_2 + \beta_p \overline{P}}, \quad \overline{I}_p = \frac{\alpha_p \overline{S}_1 \overline{P} + \beta_p \overline{S}_2 \overline{P}}{\mu_I + \theta}$$

where $\overline{P}$ is the positive root of Eq. 3.9. Using Descartes' sign rules for the polynomial (3.9), the number of positive solutions is summarized in Table 3.

As illustrated in Figure 6 (a), when $\mathcal{R} \geq 1$, there is a unique positive solution that is stable, while the DFE loses stability and becomes unstable. In Figure 6 (b), when $\mathcal{R} \leq 1$, optimal production is achieved, whereas when $\mathcal{R} \geq 1$, production decreases exponentially.

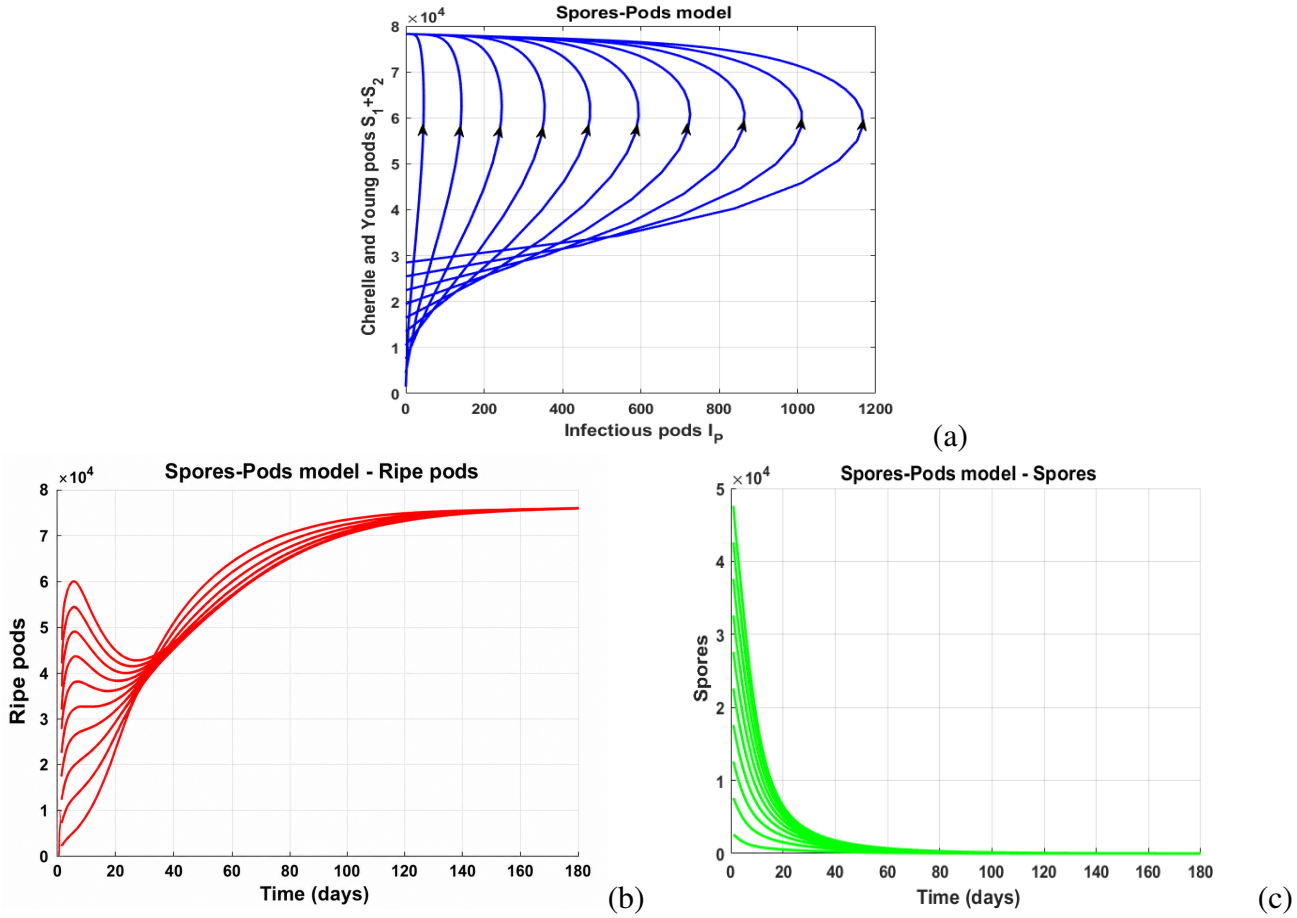


**Figure 5.** Numerical simulations for System (3.3) when $\mathcal{R} = 0.8668$; $\eta = 0.008$ and all other parameter values are shown in Table 2. (a) Phase portrait $S_1 + S_2$ versus $I_p$; (b) ripe pods $S_3$; (c) spores $P$.

**Theorem 3.** *When $\mathcal{R} \geq 1$, System (3.3) admits a unique endemic equilibrium that is locally asymptotically stable.*

**Proof**: To analyze the stability of the endemic equilibrium in relation to $\mathcal{R}$, we use Theorem 6, provided in Appendix B.

Figure 7 presents the trajectories of System (3.3) when $\mathcal{R} > 1$. It is evident from this figure that the trajectories converge to the endemic equilibrium point, as demonstrated in Theorem 3. This indicates that the disease persists within the plantation, leading to significant production losses.

### 3.2.3. Estimation of production losses caused by black pod rot disease

Herein, we present and discuss numerical simulations that highlight the production losses caused by black pod disease.

**Table 3.** Number of positive Ssolutions of Equation (3.9) using Descartes' rule for polynomials.

| $a_2$ | $a_1$ | $a_0$ | $\mathcal{R}$ | Number of positive solutions |
|---|---|---|---|---|
| + | − | + | $\mathcal{R} < 1$ | No or two positive solutions |
| + | + | + | $\mathcal{R} < 1$ | No positive solution |
| + | − | − | $\mathcal{R} > 1$ | One positive solution |
| + | + | − | $\mathcal{R} > 1$ | One positive solution |

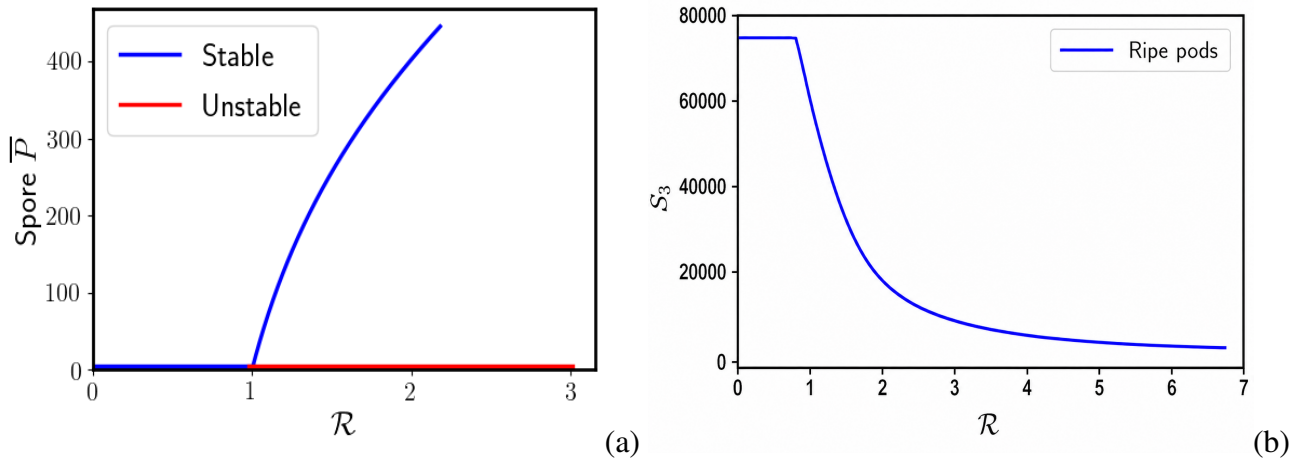


(a) (b)

**Figure 6.** Bifurcation diagram illustrating the relationship between the basic reproduction number $\mathcal{R}$ and (a) the stability of $\bar{P}$ and (b) the cocoa production $S_3$.

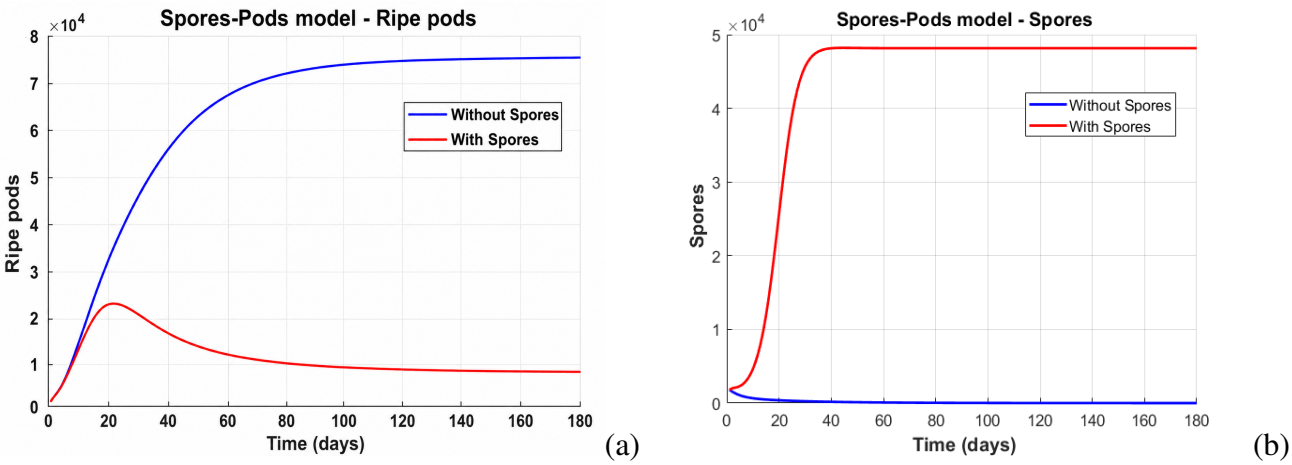


(a) (b)

**Figure 8.** Evolution of ripe pods and spores with and without black pod disease in the plot.

Figure 8 illustrates the time evolution of ripe pods both with and without black pod disease throughout the growth season. As anticipated, the number of harvested pods decreases significantly due to the disease. To quantify these results, we will summarize the data in Table 4 to estimate the production losses of cocoa within the plot.

Table 4 presents a comparison of the number of ripe pods in the presence and absence of black pod

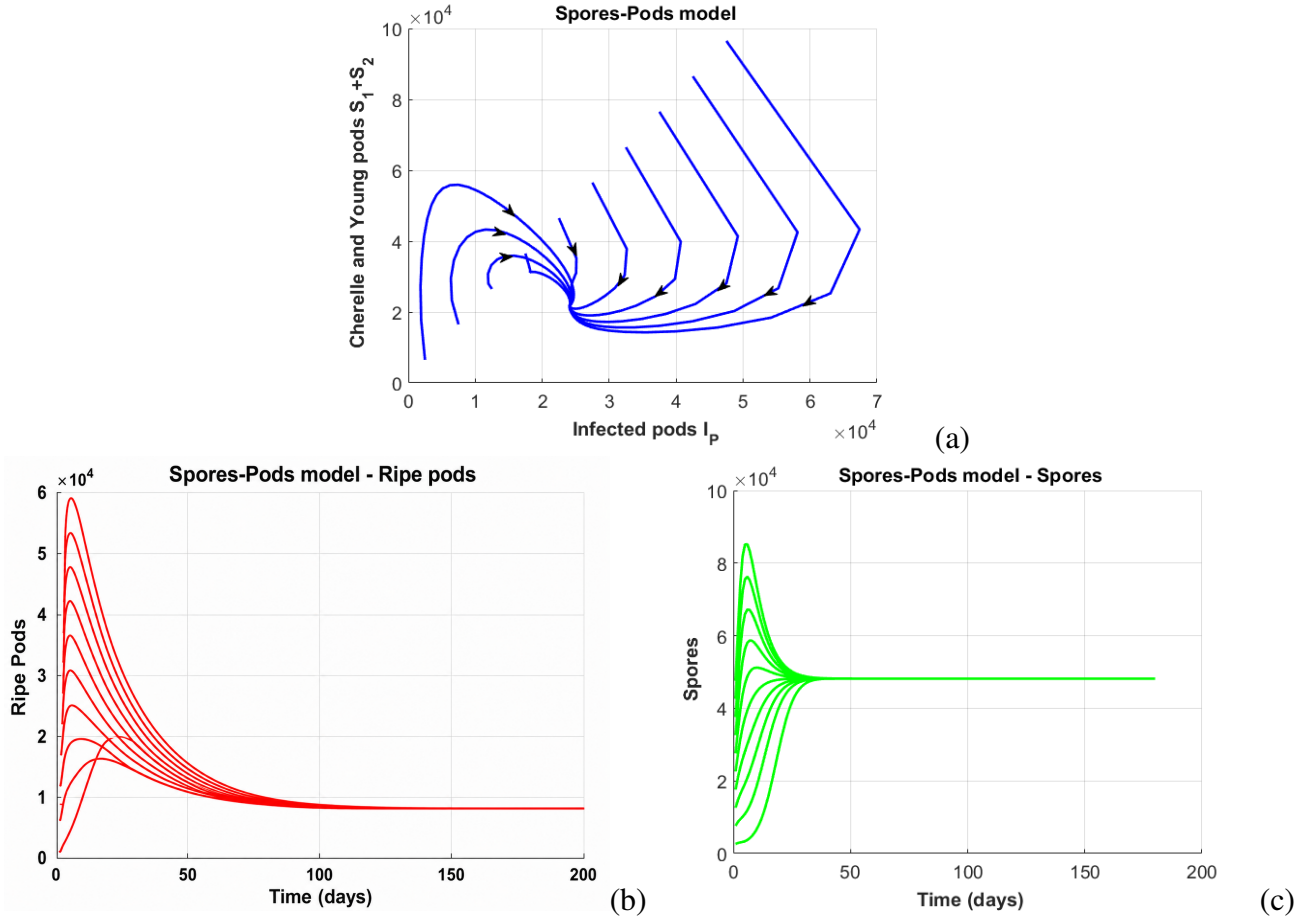


**Figure 7.** Numerical simulations of System (3.3) when $\mathcal{R} = 1.9383$. Parameter values are shown in Table 2. (a) Phase portrait for cherelle and young pods ($S_1 + S_2$) versus infected pods ($I_p$). (b) ripe pods ($S_3$). (c) spores ($P$).

disease. From this table, it is evident that the production loss is approximately 88.94%.

**Table 4.** Estimation of production losses.

| | Production without disease | Production with disease | Losses |
|---|---|---|---|
| Ripe pods | 76,000 | 8,400 | 88.94% |

The production losses due to black pod disease are substantial within a cocoa plantation. It is crucial to identify strategies to reduce the spread of this disease to enhance production in the plantation. Thus, improving phytosanitary control is essential.

Figure 9 shows the evolution of ripe pods for various values of the phytosanitary control parameter $\theta$. We observe that when the control is high, production increases. According to [25], this parameter varies within the interval $[0, 0.8]$. Numerical simulations demonstrate that when this parameter is optimal ($\theta = 0.8$), production losses are estimated to be 60%.

Black pod rot disease is a highly detrimental condition for cocoa, potentially leading to total production loss. Therefore, it is vital to manage this disease promptly upon the appearance of the first

symptoms to prevent its spread throughout the plantation. Once the disease has become widespread, control measures may only mitigate damage, and optimal production will no longer be achievable.

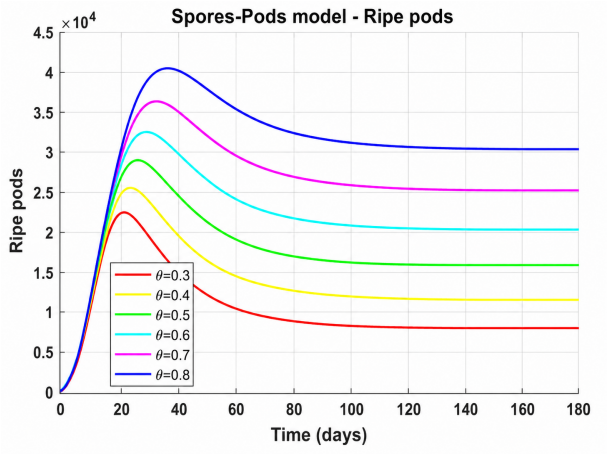


**Figure 9.** Evolution of ripe pods with various values of the phytosanitary control parameter.

### *3.3. Miridae–pods model*

Here, we study the Miridae–pods model. By setting $I_p = P = 0$ in Model (3.2), the Miridae–pods model is governed by the following differential system:

$$\begin{cases} \dot{S}_1 &= \Lambda - (\nu + \mu_1 + \alpha)\, S_1 - \alpha_m\, S_1\, M, \\ \dot{S}_2 &= \nu\, S_1 - (\gamma + \mu_2)\, S_2 - \beta_m\, S_2\, M, \\ \dot{I}_m &= \alpha_m\, S_1\, M + \beta_m\, S_2\, M - \mu_I\, I_m - d\, I_m\, M, \\ \dot{E} &= r\, b\, M\left(1 - \dfrac{E}{K}\right) - (\nu_E + \mu_E)\, E, \\ \dot{M} &= \nu_E\, E + e\, d\, I_m\, M - \mu_m\, M \quad . \end{cases} \tag{3.10}$$

#### 3.3.1. Stability of the pest–free equilibrium of the Miridae–pods sub–model (3.10)

The pest–free equilibrium of Sub-model (3.10) is obtained when there are no Miridae in the plot. Setting $E = M = 0$ and solving System (3.10) so that it is equal to zero, we compute the pest–free equilibrium point given by

$$\xi^0 = (S_1^0,\, S_2^0,\, 0,\, 0,\, 0) \quad . \tag{3.11}$$

Using the notations and method from [18], the basic offspring number is given by

$$\mathcal{N}_0 = \frac{r\, b\, \nu_E}{\mu_m\, (\nu_E + \mu_E)} \quad . \tag{3.12}$$

System (3.10) can be written in the following compact form:

$$\begin{cases} \dot{x} &= h(x, y), \\ \dot{y} &= (\tilde{F} - \tilde{V})\, y, \end{cases} \tag{3.13}$$

where $x = (S_1, S_2)^T$ represents the class of the non-infected pods, and $y = (I_m, E, M)^T$ represents the class of infected pods and the Miridae population,

$$\tilde{F} = \begin{pmatrix} 0 & 0 & \alpha_m S_1 + \beta_m S_2 \\ 0 & 0 & r\,b \\ 0 & 0 & 0 \end{pmatrix}, \quad \tilde{V} = \begin{pmatrix} \mu_I & 0 & 0 \\ 0 & \nu_E + \mu_E & 0 \\ 0 & -\nu_E & \mu_m \end{pmatrix},$$

and

$$h(x, y) = \begin{pmatrix} \Lambda - (\nu + \mu_1 + \alpha)S_1 - \alpha_m S_1 M \\ \nu S_1 - (\gamma + \mu_2)S_2 - \beta_m S_2 M \end{pmatrix}.$$

Since $\alpha_m S_1 + \beta_m S_2 \leq \alpha_m S_1^0 + \beta_m S_2^0$, System (3.13) can be bounded by the following system of equations:

$$\begin{cases} \dot{\bar{x}} = h(\bar{x}, \bar{y}), \\ \dot{\bar{y}} = (\bar{F} - \tilde{V})\,\bar{y}, \end{cases} \tag{3.14}$$

where

$$\bar{F} = \begin{pmatrix} 0 & 0 & \alpha_m S_1^0 + \beta_m S_2^0 \\ 0 & 0 & r\,b \\ 0 & 0 & 0 \end{pmatrix}.$$

Thus, the dynamics of System (3.13) is derived from the dynamics of System (3.14). Moreover, System (3.14) is globally asymptotically stable if the spectral radius of matrix $\bar{F}\tilde{V}^{-1}$ is less than one, i.e., $\rho(\bar{F}V^{-1}) \leq 1$. A simple computation shows that $\rho(\bar{F}\tilde{V}^{-1}) = \dfrac{rb\nu_E}{\mu_m(\nu_E + \mu_E)}$. This means that the pest-free equilibrium $\xi^0$ is globally asymptotically stable when $\mathcal{N}_0 \leq 1$. We have proved the following result.

**Theorem 4.** *The pest–free equilibrium $\xi^0$ is globally asymptotically stable when $\mathcal{N}_0 \leq 1$.*

Figure 10 presents the sensitivity analysis of the basic offspring number $\mathcal{N}_0$ and the optimal production $S_3$. We observe that $\mathcal{N}_0$ is significantly affected by parameters $r$, $b$, and $\nu_E$, which have positive effects, as well as $\mu_m$ and $\mu_E$, which have negative effects. The production $S_3$ is more influenced by $\Lambda$ and $\nu$, which have positive effects, and $\mu_3$ and $\gamma$, which have negative effects. For the numerical simulations, we selected the following arbitrary initial conditions: $S_1(0) = 1000$, $S_2(0) = 500$, $S_3(0) = I_m(0) = 0$, $E(0) = 0$, and $M(0) = 960$, as recommended by [26].

Figure 11, on Page 2674, illustrates the trajectories of System (3.10). From this figure, it is evident that the trajectories of System (3.10) converge to the pest-free equilibrium $\xi^0$, as demonstrated in Theorem 4. This convergence indicates that the pest disappears within the cocoa plot, allowing for optimal production. Blue, red, cyan, and green colours represent, respectively, the phase plane (infectious pods, cherelles, and young pods), the ripe pods, eggs, and Miridae evolution.

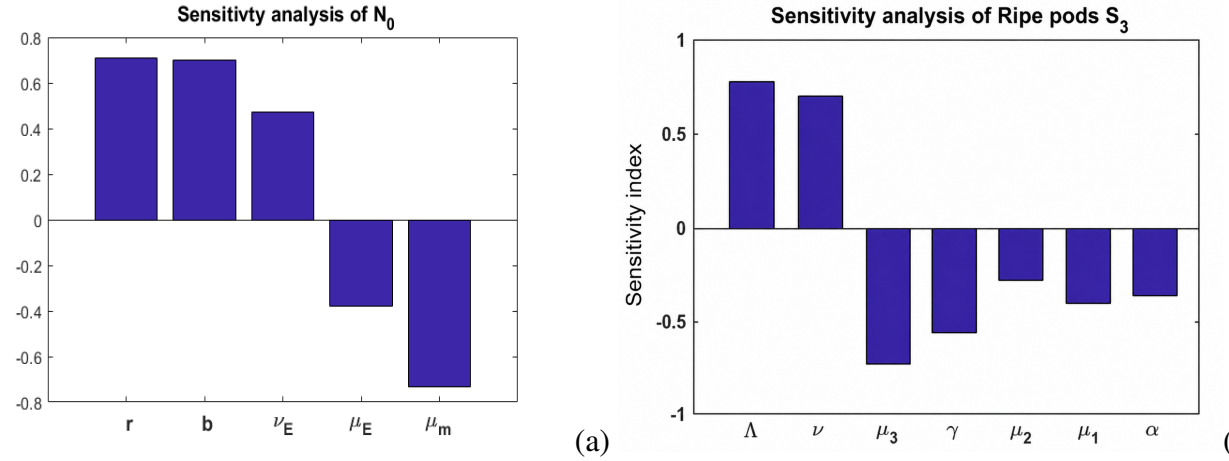


(a) (b)

**Figure 10.** Sensitivity analysis of the basic offspring number $\mathcal{N}_0$ and the production of ripe pods $S_3$.

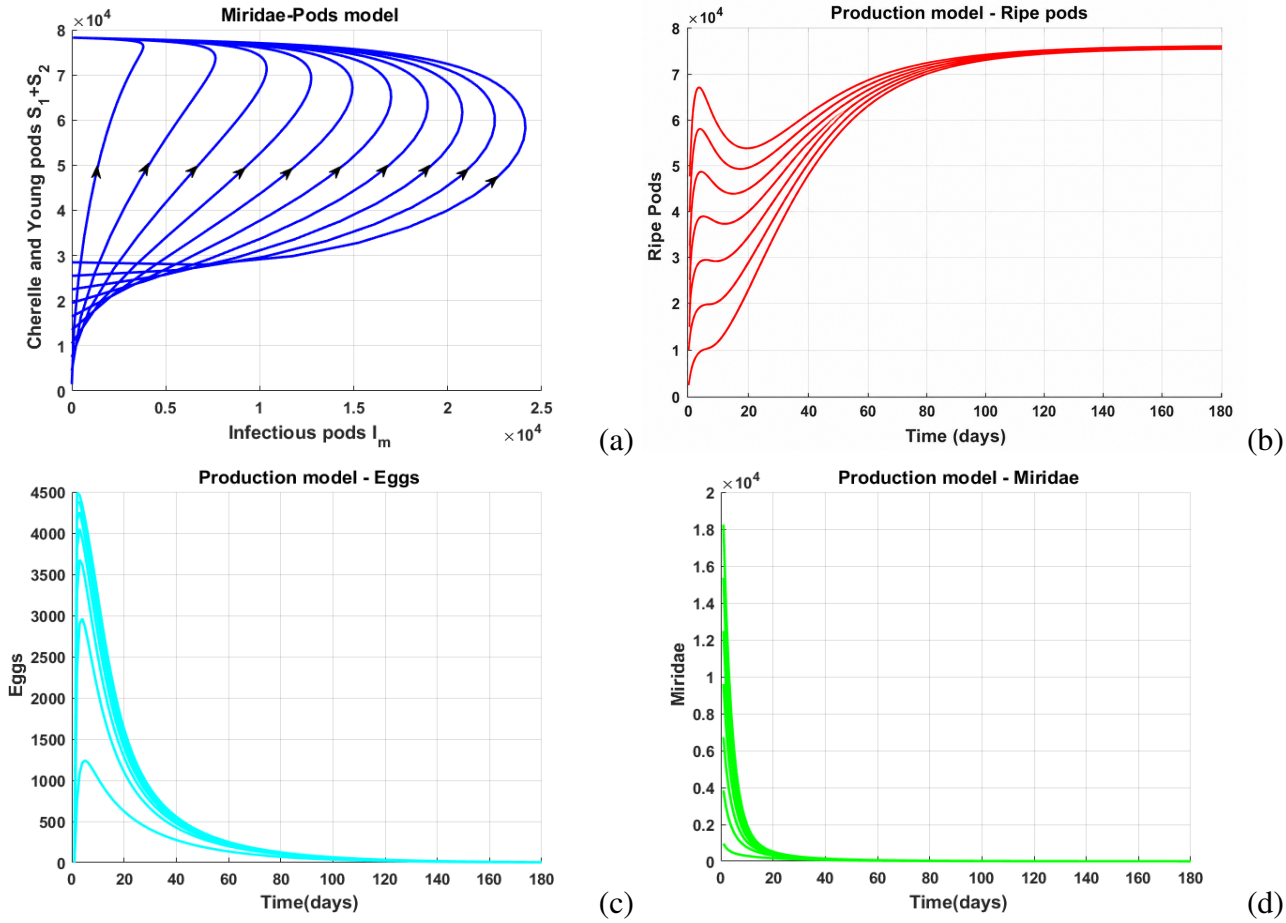


(a) (b) (c) (d)

**Figure 11.** Numerical simulations for System (3.10) when $\mathcal{N}_0 = 0.8992 \leq 1$; $b = 2$; $\mu_E = 0.2$; $\mu_m = 0.3$; other parameter values are given in Table 2. (a) Phase portrait of $S_1 + S_2$ versus $I_m$; (b) ripe pods $S_3$; (c) eggs $E$; (d) Miridae $M$.

3.3.2. The pest equilibrium point and its stability

Let $(\tilde{S}_1, \tilde{S}_2, \tilde{I}_m, \tilde{E}, \tilde{M})$ be the endemic equilibrium of Model (3.10). The endemic equilibrium is obtained by setting System (3.10) equal to zero, leading to the following polynomial equation:

$$b_4 M^4 + b_3 M^3 + b_2 M^2 + b_1 M + b_0 = 0 \tag{3.15}$$

where

$$\begin{aligned}
b_4 =& r\,b\,d\,\mu_m\,\alpha_m\,\beta_m,\\
b_3 =& r\,b\,\mu_m\,d\,(\alpha_m\,(\gamma+\mu_2)+\beta_m\,(\nu+\mu_1+\alpha))+\alpha_m\,\beta_m\,[r\,b\,\mu_m\,\mu_I+d\,K\,\mu_m\,(\nu_E+\mu_E)\,(1-\mathcal{N}_0)],\\
b_2 =& [\beta_m\,(\nu+\mu_1+\alpha)+\alpha_m\,(\gamma+\mu_2)][d\,K\,\mu_m\,(\nu_E+\mu_E)\,(1-\mathcal{N}_0)+r\,b\,\mu_m\,\mu_I]-\Lambda\,e\,d\,\beta_m\\
&+r\,b\,\mu_m\,(\gamma+\mu_2)\,(\nu+\mu_1+\alpha),\\
b_1 =& K\,\mu_m\,(\nu_E+\mu_E)\,(1-\mathcal{N}_0)\,\mu_I\,[\beta_m\,(\nu+\mu_1+\alpha)+\alpha_m\,(\gamma+\mu_2)]-(e\,d\,\Lambda\,\nu+\Lambda\,(\gamma+\mu_2))\\
&+(\nu+\mu_1+\alpha)\,(\gamma+\mu_2)\,[r\,b\,\mu_m\,\mu_I+d\,K\,\mu_m\,(\nu_E+\mu_E)\,(1-\mathcal{N}_0)],\\
b_0 =& K\,\mu_m\,(\nu_E+\mu_E)\,\mu_I\,(\nu+\mu_1+\alpha)\,(\gamma+\mu_2)\,(1-\mathcal{N}_0)\quad .
\end{aligned}$$

To apply Descartes' rule of signs for the polynomial $b_4M^4+b_3M^3+b_2M^2+b_1M+b_0 = 0$, we analyze the number of sign changes in the sequence of coefficients $b_4, b_3, b_2, b_1, b_0$. We then identify the number of sign changes in this sequence, where a sign change occurs when one coefficient is positive and the next is negative, or vice versa. Descartes' rule of signs states that the number of positive real roots is either equal to the number of sign changes in the sequence or less than that number by an even integer.

For example, if the sequence of signs is $+,-,+,-$, there are three sign changes, indicating that the number of positive real roots could be three, one, or none. To determine the exact number of positive solutions, we compute the coefficients based on the parameter values and apply Descartes' rule. The results are presented in Table 5, showing the number of positive roots for different parameter configurations. Figure 12 shows that when $\mathcal{N}_0 \geq 1$, there is a unique positive solution which is stable,

**Table 5.** Number of positive solutions of Equation (3.15) using Descartes' rule of signs.

| $b_4$ | $b_3$ | $b_2$ | $b_1$ | $b_0$ | $\mathcal{N}_0$ | Number of positive solutions |
|---|---|---|---|---|---|---|
| + | − | + | + | + | $\mathcal{N}_0 < 1$ | No or two positive solutions |
| + | − | + | − | + | $\mathcal{N}_0 < 1$ | Four or two positive solutions |
| + | − | − | + | + | $\mathcal{N}_0 < 1$ | No or two positive solutions |
| + | − | − | − | + | $\mathcal{N}_0 < 1$ | No or two positive solutions |
| + | + | + | + | − | $\mathcal{N}_0 > 1$ | One positive solution |
| + | + | + | − | − | $\mathcal{N}_0 > 1$ | One positive solution |
| + | + | − | + | − | $\mathcal{N}_0 > 1$ | One or three positive solutions |
| + | + | − | − | − | $\mathcal{N}_0 > 1$ | One positive solution |

and the pest-free equilibrium changes its stability, becoming unstable.
Explicitly, endemic equilibrium $(\tilde{S}_1, \tilde{S}_2, \tilde{I}_m, \tilde{E}, \tilde{M})$ of Model (3.10) is given by:

$$\tilde{S}_1 = \frac{\Lambda}{\nu+\mu_1+\alpha+\alpha_m\tilde{M}},\ \tilde{S}_2 = \frac{\nu\tilde{S}_1}{\gamma+\mu_2+\beta_m\tilde{M}},\ \tilde{I}_m = \frac{\alpha_m\tilde{S}_1\tilde{M}+\beta_m\tilde{S}_2\tilde{M}}{\mu_I+d\tilde{M}},\ \tilde{E} = \frac{rb\tilde{M}(K-\tilde{E})}{K(\nu_E+\mu_E)}$$

where $\tilde{M}$ is the positive root of Eq. (3.15).

**Theorem 5.** *When $\mathcal{N}_0 \geq 1$, System (3.10) admits a unique endemic equilibrium, which is locally asymptotically stable.*

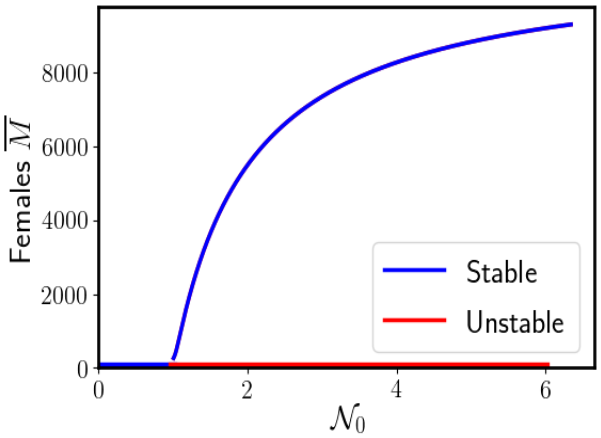


**Figure 12.** Bifurcation diagram showing the behavior of $\bar{M}$ (on the y-axis) as a function of $\mathcal{N}_0$.

Figure 13 presents the trajectories of System (3.10) with various initial conditions when $\mathcal{N}_0 > 1$. The figure clearly shows that these trajectories converge to the pest equilibrium point, as established in Theorem 5. This indicates that the pest persists within the cocoa plot, leading to production losses.

### 3.3.3. Estimation of production losses caused by Miridae

This section presents and discusses numerical simulations that highlight the production losses caused by Miridae within a plantation.

Figure 14 illustrates the time evolution of ripe pods with and without Miridae during a growth season. As expected, the number of harvested pods decreases significantly. These results are summarized in Table 6, which presents the production of pods with and without Miridae, along with the calculated losses, indicating that the production losses are approximately 34.21%.

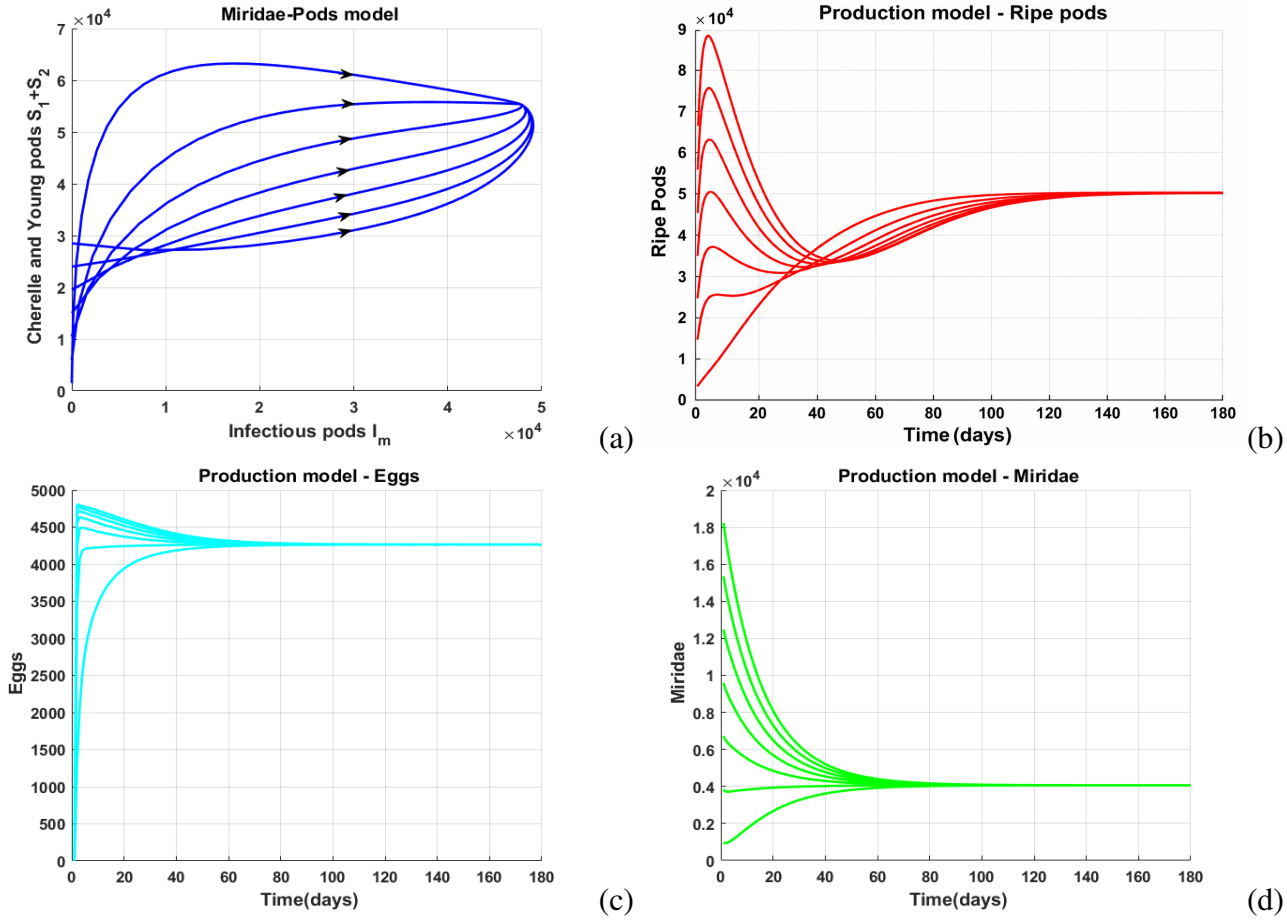


**Figure 13.** Numerical simulations for System (3.10) when $\mathcal{N}_0 = 6.1867 \geq 1$. Parameter values are shown in Table 2. (a) Phase portrait of $S_1 + S_2$ versus $I_m$; (b) ripe pods $S_3$; (c) eggs $E$; (d) Miridae $M$.

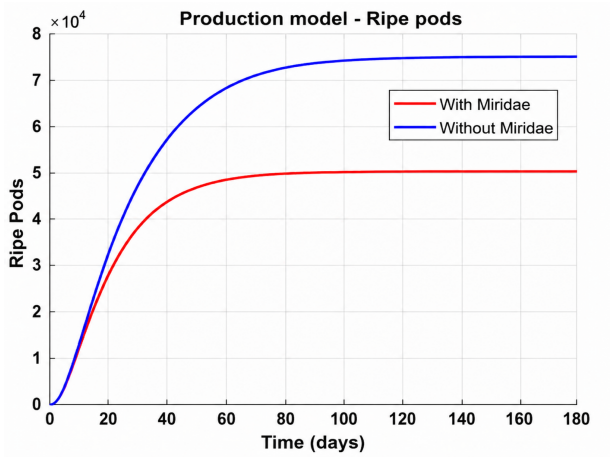


**Figure 14.** Ripe pods with and without Miridae in the plot: Without Miridae (blue line) and With Miridae (red line).

**Table 6.** Estimation of production losses due to Miridae infestation.

| | Production without Miridae | Production with Miridae | Losses |
|---|---|---|---|
| Ripe pods | 76,000 | 50,000 | 34.21% |

### *3.4. Co–infection model: Spores–Pods, and Miridae*

In this section, we present the mathematical analysis of the co-infection model described by Equation (3.2).

#### 3.4.1. Stability of the DFE of the co–infection model (3.2)

For Model (3.2), the DFE is defined as

$$DFE = (S_1^0, S_2^0, 0, 0, 0, 0, 0, 0), \tag{3.16}$$

where $S_1^0$ and $S_2^0$ are specified in Eq. (3.4). The stability of the DFE is governed by the basic reproduction number. Following the work of Van den Driessche and Watmough [18], the basic reproduction number for Model (3.2) is given by

$$\mathcal{R}_0 = \max\{\mathcal{R},\ \mathcal{N}_0\}, \tag{3.17}$$

where $\mathcal{R}$ and $\mathcal{N}_0$ represent the pods–spores and pods–Miridae–induced basic reproduction and basic offspring numbers, respectively. These quantities are defined as follows:

$$\mathcal{R} = \left(\frac{\eta\,\sigma\,\Lambda\,(\beta_p\,\nu + \alpha_p\,(\gamma + \mu_2))}{\mu_p\,(\mu_I + \theta)\,(\mu_2 + \gamma)\,(\nu + \mu_1 + \alpha)}\right)^{1/2} \quad \text{and} \quad \mathcal{N}_0 = \frac{r\,b\,\nu_E}{\mu_m\,(\nu_E + \mu_E)}. \tag{3.18}$$

Using Theorem 2 from Van den Driessche and Watmough [18], we establish the following result.

**Lemma 3.** *The DFE of Model (3.2) is locally asymptotically stable whenever* $\mathcal{R}_0 < 1$ *and unstable otherwise.*

#### 3.4.2. Co–existence thresholds

In this section, we derive the expressions for the regions of stability boundary equilibria. Two coexistence thresholds must be calculated: The first separates the region where only black pod disease persists from the region of coexistence, while the second marks the shift from coexistence to the persistence of Miridae alone.

To derive an expression for the region of stability of the boundary equilibrium, we assess the capacity of black pod disease to invade and persist in a plot where Miridae are at equilibrium. In this context, the DFE for the Model (3.2) is given by

$$Q_M^* = (S_1^{**}, S_2^{**}, I_m^{**}, 0, 0, 0, E^{**}, M^{**}), \tag{3.19}$$

where

$$S_1^{**} = \frac{\Lambda}{\nu + \mu_1 + \alpha + \alpha_m\,M^{**}}, \quad S_2^{**} = \frac{\nu\,S_1^{**}}{\gamma + \mu_2 + \beta_m\,M^{**}},$$

$$I_m^{**} = \frac{\alpha_m S_1^{**} M^{**} + \beta_m S_2^{**} M^{**}}{\mu_I + dM^{**}}, \quad E^{**} = \frac{rbM^{**}(K - E^{**})}{K(\nu_E + \mu_E)}$$

with $M^{**}$ being the positive equilibrium of equation (3.15).

Applying the methods of Van den Driessche and Watmough [18], we find the basic reproduction number of spores in a plantation where Miridae states are fixed

$$\mathcal{R}(Q_M^*) = \frac{\eta\,\sigma\,(\alpha_p\,S_1^{**} + \beta_p\,S_2^{**})}{\mu_p\,(\mu_I + \theta)} \quad . \tag{3.20}$$

Note that $\mathcal{R}(Q_M^*)$ is independent of Miridae parameters except through the equilibrium values $S_1^{**}$ and $S_2^{**}$. This reflects the fact that Miridae affect black pod disease transmission only by reducing the susceptible pod population, not by altering spore production or infection efficiency directly. The threshold $\mathcal{R}(Q_M^*)$ serves as a threshold condition for coexistence, which is equivalent to a threshold condition for black pod disease endemicity in a plantation where Miridae are at equilibrium. When $\mathcal{R}(Q_M^*) < 1$, only Miridae persists in the plot, while for $\mathcal{R}(Q_M^*) > 1$, black pod disease can invade the plot where the Miridae states are fixed; in other words, coexistence becomes possible. Lemma 4 below expresses this result in terms of the stability for the equilibrium $Q_M^*$.

**Lemma 4.** *If $\mathcal{N}_0 > 1$, the spores-free equilibrium $Q_M^*$ is stable for $\mathcal{R}(Q_M^*) < 1$ and unstable for $\mathcal{R}(Q_M^*) > 1$.*

Figure 15 presents the solution profiles for spore-infected pods, Miridae-damaged pods, ripe pods, and co-infected pods from the System (2.1), with $\mathcal{R} = 0.5308 \leq 1$ and $\mathcal{R}(Q_M^*) = 0.4464 \leq 1$.

Figure 16 presents the solution profiles of spore-infected pods, Miridae-damaged pods, ripe pods, and co-infected pods from the System (2.1), with $\mathcal{R} = 1.9333 \geq 1$ and $\mathcal{R}(Q_M^*) = 1.6302 \geq 1$.

The black pod disease is endemic when $\mathcal{R} > 1$. We use the same reasoning as before, considering Miridae as the invading species in a plantation where black pod disease is already endemic.

Let

$$Q_p^* = (S_1^*, S_2^*, 0, 0, I_p^*, P^*, 0, 0) \quad , \tag{3.21}$$

where

$$S_1^* = \frac{\Lambda}{\nu + \mu_1 + \alpha + \alpha_p\,P^*}, \quad S_2^* = \frac{\nu\,S_1^*}{\gamma + \mu_2 + \beta_p\,P^*}, \quad I_p^* = \frac{\alpha_p S_1^* P^* + \beta_p S_2^* P^*}{\mu_I + \theta},$$

with $P^*$ being the positive equilibrium of Equation (3.9). This represents the DFE of Model (3.2) when the black pod disease is endemic in the plot. We will now compute the region of stability of the boundary equilibrium $Q_p^*$. This equilibrium exists and is unique when $\mathcal{R} > 1$.

Applying the method of Van den Driessche and Watmough [18], we find the basic offspring number of the Miridae in a plantation where the black pod disease is fixed

$$\mathcal{N}_0(Q_p^*) = \frac{r\,b\,\nu_E}{\mu_m\,(\nu_E + \mu_E)} \quad . \tag{3.22}$$

Note that the expression for $\mathcal{N}_0(Q_p^*)$ is similar to that for $\mathcal{N}_0$ in Eq. (3.12) because Miridae's reproduction depends on pod availability but not directly on the black pod disease status of pods; infected pods remain suitable for oviposition under our model assumptions. Miridae can invade the plot where the black pod disease is fixed whenever $\mathcal{N}_0 > 1$. The corresponding result for the stability of equilibrium $Q_p^*$ is expressed in Lemma 5.

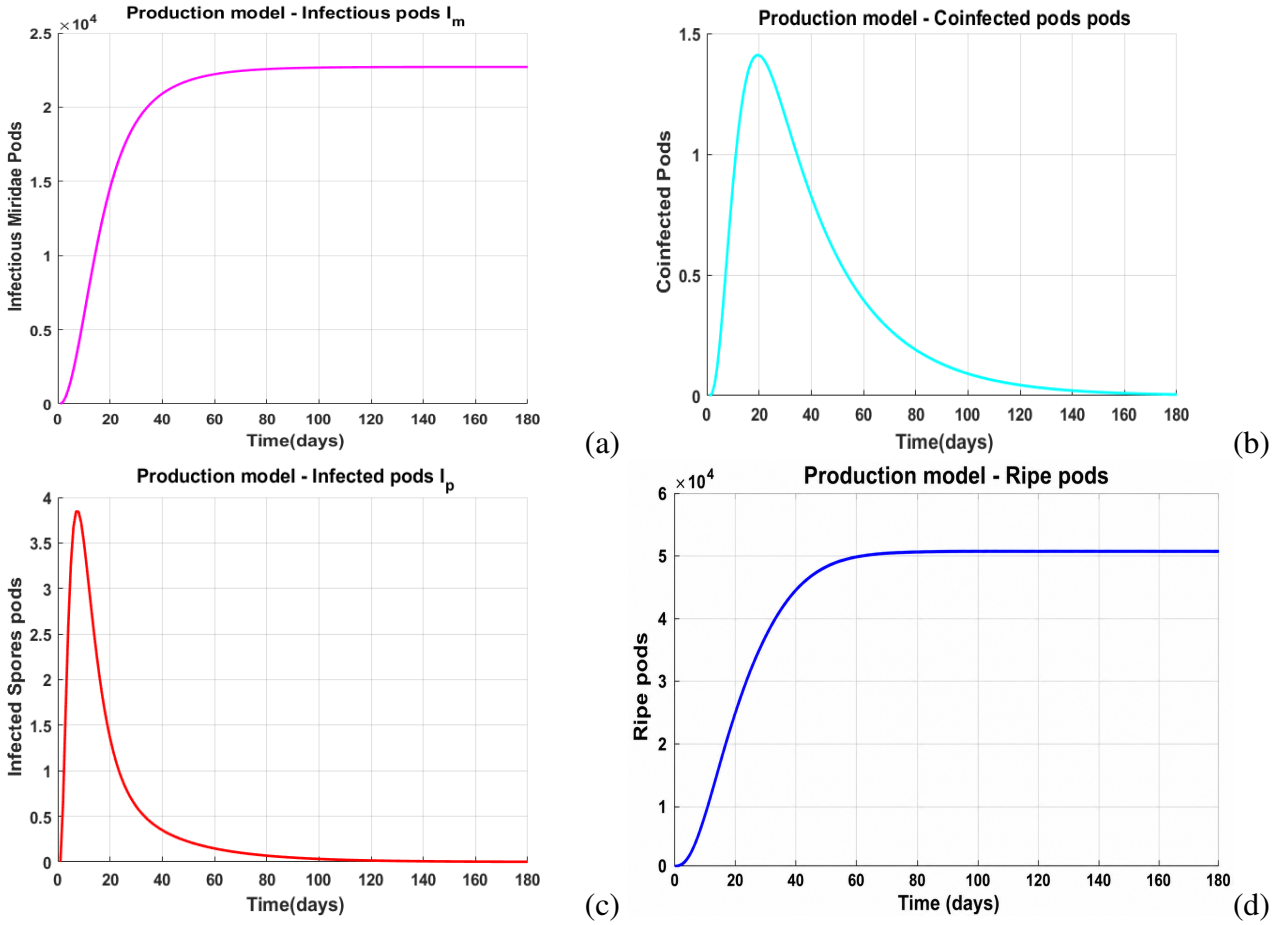


**Figure 15.** Numerical simulations for system (2.1) when $\mathcal{R} = 0.5308$, $\mathcal{R}(Q_M^*) = 0.4464$, $\mathcal{N}_0 = 6.7943$ (resulting in $\mathcal{R}_0 = 6.7943 > 1$) (a) Miridae-damaged pods $I_m$; (b) Co-infected pods $I_{mp}$; (c) Spore-infected pods $I_p$; (d) Ripe pods $S_3$. Parameters values are shown in Table 2.

**Lemma 5.** *If $\mathcal{R} > 1$, the Miridae-free equilibrium $Q_p^*$ is stable for $\mathcal{N}_0 < 1$ and unstable for $\mathcal{N}_0 > 1$.*

Figure 17 presents the solution profiles of spore-infected pods, Miridae-damaged pods, ripe pods, and co-infected pods of System (2.1), with $\mathcal{N}_0 = 0.8992 \leq 1$ and $\mathcal{R} = 1.9333 > 1$.

Figure 18 illustrates the time evolution of ripe pods with and without coinfection during a growth season. In Figure 18 (a), we first consider the infection due to black pod disease (blue color) and then the coinfection (red colour). Figure 18 (b) presents the time evolution of ripe pods with and without co-infection with Miridae. It has been shown that co-infection contributes to reduce the number of ripe pods.

### *3.5. Interactions between black pod rot disease and Miridae infestation: Impacts on cocoa yield*

#### 3.5.1. Quantifying production losses under co–infection

To assess the influences between black pod rot disease and Miridae infestation, we evaluate plantation's productivity under co-infection conditions. We consider the impact of black pod rot on Miridae

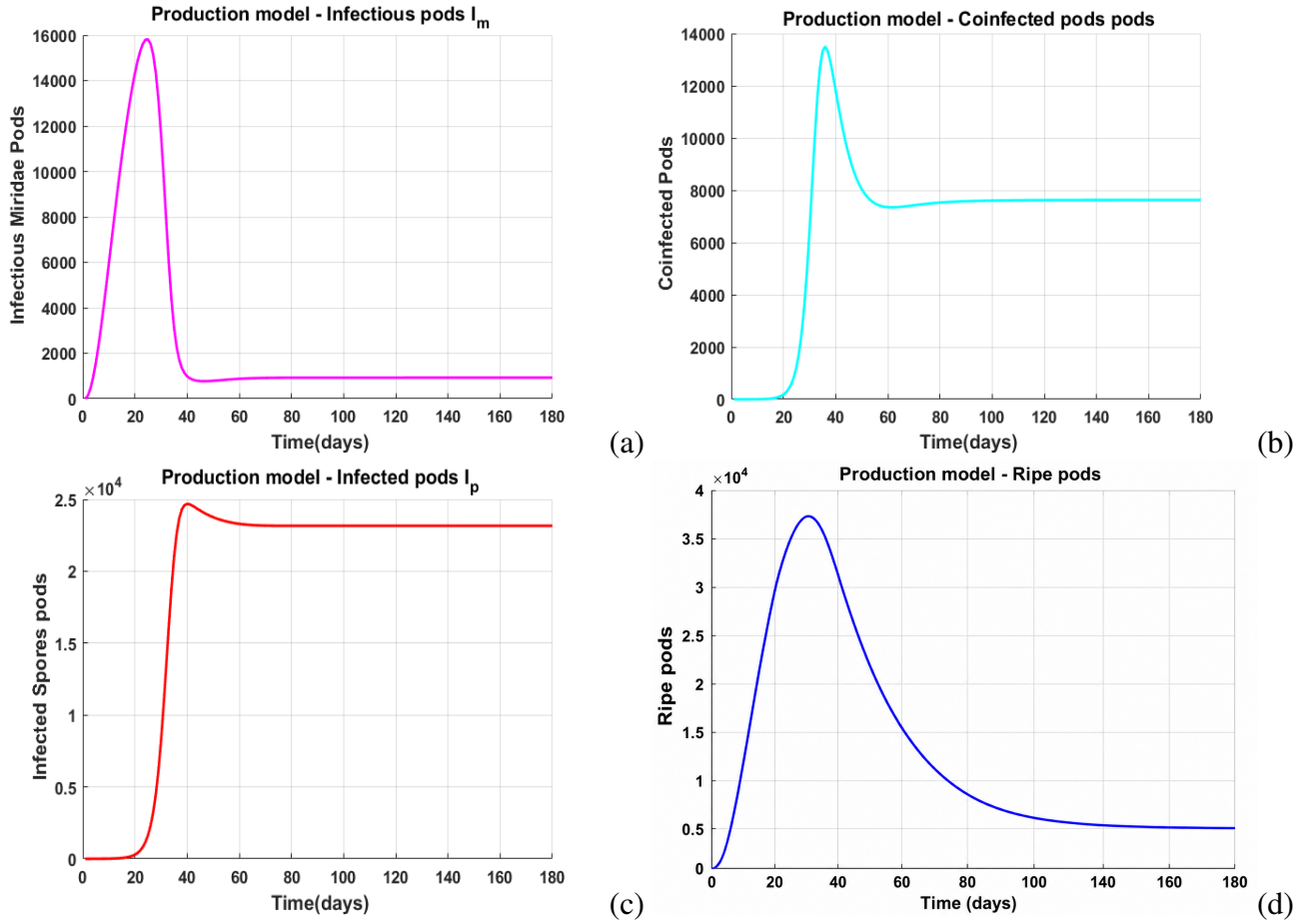


**Figure 16.** Numerical simulations for System (2.1) when $\mathcal{R} = 1.9333$, $\mathcal{R}(Q_M^*) = 1.6302$, $\mathcal{N}_0 = 6.7943$ (so that $\mathcal{R}_0 = 6.7943 > 1$). (a) Miridae-damaged pods $I_m$; (b) co-infected pods $I_{mp}$; (c) spore-infected pods $I_p$; (d) ripe pods $S_3$.

(through reduced susceptible pod availability). The estimated production losses highlight the devastating synergy between Miridae and black pod rot on cocoa yield. When both are present, they can induce near-total production collapse. Specifically, co-infection results in losses exceeding 93%, compared with approximately 88.94% for black pod rot alone and 34.21% for Miridae alone. These findings underscore the critical need for integrated management strategies targeting both pests and pathogens to optimize cocoa production.

### 3.5.2. Formulation of impulsive control strategies

A feasible control strategy includes the following measures: (i) Removal of infected pods to limit direct transmission of black pod rot disease; (ii) Application of fungicides to eliminate spores and thus reduce indirect transmission; and (iii) Use of insecticides to suppress Miridae populations. These control actions increase the parameters $\theta$, $\mu_p$, and $\mu_M$, representing the rates of infected pod removal, spore inactivation, and Miridae mortality, respectively. Following [20], we incorporate these actions using impulsive differential equations. For each control variable $\phi \in \{\theta^*, \mu_p^*, \mu_M^*\}$, we define two parameters: $\overline{\phi}$ (empirical mean) and $r_\phi$ (growth rate). Defining $\theta^* = 1 - \theta$, $\mu_p^* = 1 - \mu_p$, and $\mu_M^* = 1 - \mu_M$, control

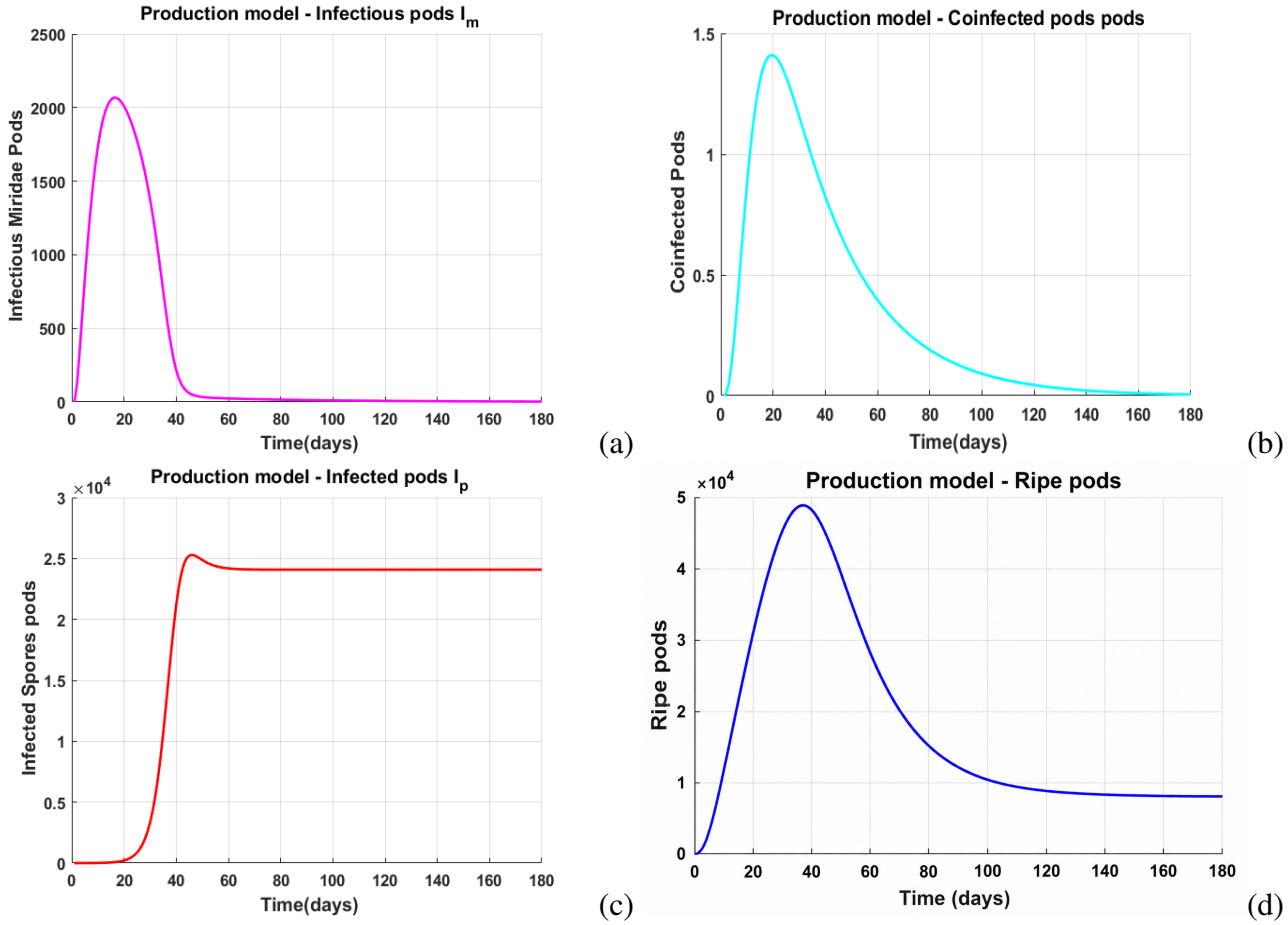


**Figure 17.** Numerical simulations for System (2.1) when $\mathcal{R} = 1.9333$, $\mathcal{R}(Q_M^*) = 1.6302$, and $\mathcal{N}_0 = 0.8992$ (so that $\mathcal{R}_0 = 1.9333 > 1$). (a) Miridae-damaged pods $I_m$; (b) co-infected pods $I_{mp}$; (c) spore-infected pods $I_p$; (d) ripe pods $S_3$.

actions temporarily reduce $\theta^*$, $\mu_p^*$, and $\mu_M^*$. We consider two parameters that drive its temporal evolution: $\overline{\phi}$, the empirical mean value, and $r_\phi$, the growth rate. Among several empirical formulations, we adopt the simplest ordinary differential equation as follows:

$$\begin{cases} \dfrac{d\phi}{dt} &= r_\phi\,(\overline{\phi} - \phi), \\ \phi(0) &= \phi_0. \end{cases} \tag{3.23}$$

Assuming $r_\phi > 0$, the analytical solution is:

$$\phi(t) = \overline{\phi} - (\overline{\phi} - \phi_0)\, e^{-r_\phi\, t} \tag{3.24}$$

Thus, $\phi(t)$ converges to $\overline{\phi}$. Let $\delta$ be the proportion of farmers applying control measures. Control efficiency is assumed to increase with $\delta$. Control actions are applied instantaneously at discrete times:

$$\Delta\phi(t_i) = -\varphi(\delta)\,\phi(t_i) \tag{3.25}$$

where $\varphi(\delta)$ is an increasing function with $\varphi(0) = 0$ and $0 < \varphi(1) < 1$ (imperfect control). It can be linear ($\varphi(x) = ax$, $a \in (0, 1)$) or nonlinear ($\varphi(x) = \frac{ax}{1+ax}$, $a > 0$) where $a$ is a parameter that can be

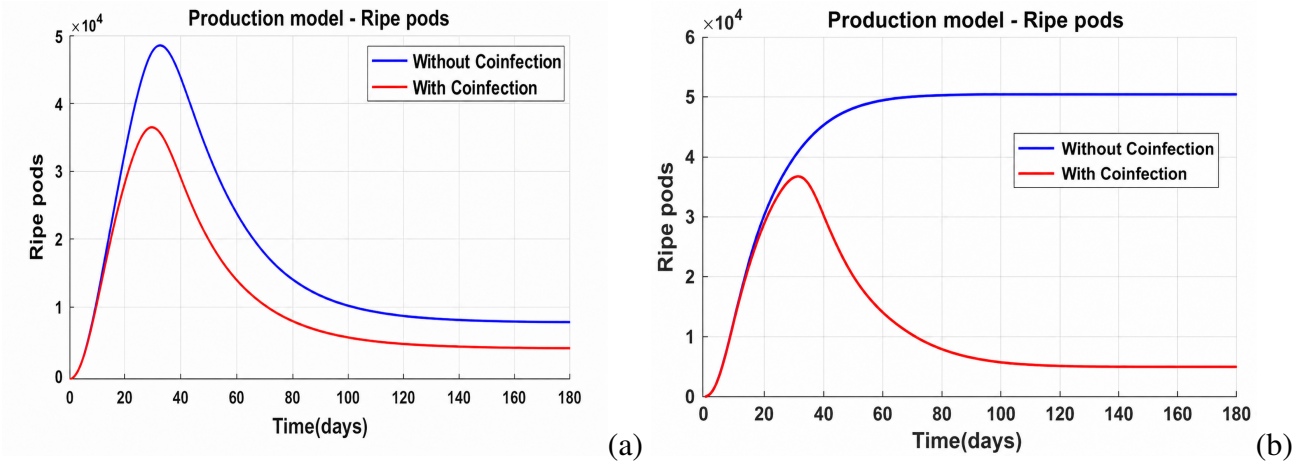


**Figure 18.** Estimation of production losses due to co-infection. Under co-infection, production losses exceed 90% in our simulations, approaching near–total loss when both pathogens are present.

related to the rate of efficacy. The resulting impulsive system is:

$$\begin{cases} \dfrac{d\phi}{dt} &= r_\phi\,(\overline{\phi} - \phi), \\ \Delta\phi(t_0 + n\tau) &= -\varphi(\delta)\,\phi(t_0 + n\tau), \quad n = 0, 1, 2, \ldots \\ \phi(0) &= \phi_0. \end{cases} \tag{3.26}$$

According to the theory of impulsive differential equations [21], Eq. (3.26) is well defined and has a unique positive periodic solution $\phi_{per}(t)$. Suppose $\delta$ constant and replacing the constant parameters $\theta$, $\mu_p$, $\mu_M$ with $\theta_{per}(t) = 1 - \theta^*_{per}(t)$, $\mu_{p_{per}}(t) = 1 - \mu^*_{p_{per}}(t)$, and $\mu_{M_{per}}(t) = 1 - \mu^*_{M_{per}}(t)$ yields the full time-dependent model (System (3.28)).

**Proposition 1.** *The periodic function*

$$\phi_{per}(t) = \begin{cases} \overline{\phi} - (\overline{\phi} - \phi_0)\, e^{-r_\phi t}, & t \in [0, t_0] \\ \overline{\phi} - (\overline{\phi} - (1 - \varphi(\delta))\,\phi((n-1)\tau + t_0))\, e^{-r_\phi (t - (n-1)\tau - t_0)}, & t \in ((n-1)\tau + t_0,\, n\tau + t_0],\ n = 1, 2, \ldots \end{cases} \tag{3.27}$$

*is the solution of Eq. (3.26).*

We will use each periodic solution $\theta^*_{per}$, $\mu^*_{p_{per}}$, and $\mu^*_{M_{per}}$ of (3.26) in System (2.1). Replacing the constant parameters $\theta$, $\mu_p$, and $\mu_M$ by the functions $\theta_{per}(t)$ ($\theta_{per}(t) = 1 - \theta^*_{per}(t)$), $\mu_{p_{per}}(t)$ ($\mu_{p_{per}}(t) = 1 - \mu^*_{p_{per}}(t)$), $\mu_{M_{per}}(t)$ ($\mu_{M_{per}}(t) = 1 - \mu^*_{M_{per}}(t)$) respectively, we obtain the following system of differential

equations refering to the time-dependent controlled model:

$$\begin{cases} \dot{S}_1 &= \Lambda - (\nu + \mu_1 + \alpha)\, S_1 - \alpha_m\, S_1\, M - \alpha_p\, S_1\, P, \\ \dot{S}_2 &= \nu\, S_1 - (\gamma + \mu_2)\, S_2 - \beta_m\, S_2\, M - \beta_p\, S_2\, P, \\ \dot{I}_m &= \alpha_m\, S_1\, M + \beta_m\, S_2\, M - \mu_I\, I_m - \beta_p\, I_m\, P - d\, I_m\, M, \\ \dot{I}_{mp} &= \beta_p\, I_m\, P - \mu_I\, I_{mp} - \theta_{per}(t)\, I_{mp}, \\ \dot{I}_p &= \alpha_p\, S_1\, P + \beta_p\, S_2\, P + \beta_p\, I_m\, P - (\mu_I + \theta_{per}(t))\, I_p, \\ \dot{S}_3 &= \gamma\, S_2 - \mu_3\, S_3, \\ \dot{P} &= \eta\, \sigma\, (I_p + I_{mp}) - \mu_{p_{per}}(t)\, P, \\ \dot{E} &= r\, b\, M \left(1 - \frac{E}{K}\right) - (\nu_E + \mu_E)\, E, \\ \dot{M} &= \nu_E\, E + e\, d\, I_m\, M - \mu_{M_{per}}(t)\, M. \end{cases} \tag{3.28}$$

3.5.3. Control scenarios and numerical results

For the simulations, we used: $\tau = 180$ days (control interval), $t_0 = 10$ days, $\delta = 0.7$, $a = 0.8$, $r_\phi = 0.1$, $\overline{\theta} = 0.3$, $\overline{\mu}_p = 0.02$, and $\overline{\mu}_M = 0.07$. We present three control scenarios, illustrated in Figures 19 and 20.

- **Scenario 1: Control of black pod disease only.**
  We simulate a situation where the control measures target solely the progression of black pod rot disease. Phytosanitary control is applied by removing infected pods from the plantation to limit direct disease transmission. Additionally, chemical fungicides are used to suppress *Phytophthora megakarya*, the main causal agent of black pod rot in Central and West Africa. In this case, the parameters $\theta_{per}$ and $\mu_{p_{per}}$ in Model (3.28) are considered, while all other parameters remain unchanged when $\mathcal{R}$ and $\mathcal{N}_0$ exceed one.
- **Scenario 2: Control of Miridae only.**
  Here, we focus on reducing Miridae populations within the plantation. This strategy aims to minimize the damage caused by Miridae feeding and, over time, enhance the overall health of the cocoa trees. We assume that Miridae control is achieved through the application of insecticides every $\tau$ days, effectively decreasing Miridae's abundance. In this case, the parameter $\mu_{M_{per}}$ is used in Model (3.28), with all other parameters remaining constant when $\mathcal{R}$ and $\mathcal{N}_0$ are greater than one.
- **Scenario 3: Combined control of black pod rot and Miridae.**
  In this scenario, both phytosanitary and Miridae control measures are applied simultaneously. The objective is to maximize cocoa production by jointly reducing Miridae populations and removing pods infected by black pod rot every $\tau$ days. Consequently, both Miridae's abundance and the

number of infected pods decrease at each intervention, leading to improved overall yield.

**Single-threat scenarios:** Figure 19(a) depicts the first situation, where the plantation is affected only by Miridae infestations. An impulsive control strategy is implemented by applying insecticides at specific time intervals. The blue curve represents cocoa production in the absence of Miridae, while the magenta curve corresponds to production under Miridae infestation with control and the red curve shows the production without any control. A clear improvement in production is observed when control measures are applied.

The second situation, shown in Figure 19(b), considers a plantation affected only by black pod disease. In this case, control actions consist of reducing spore concentrations through fungicide application and removing infected pods (phytosanitary control). The blue curve represents optimal production without disease, the magenta curve shows production under black pod infection with control, and the red curve shows the production without control. The results demonstrate a significant increase in production when control strategies are implemented.

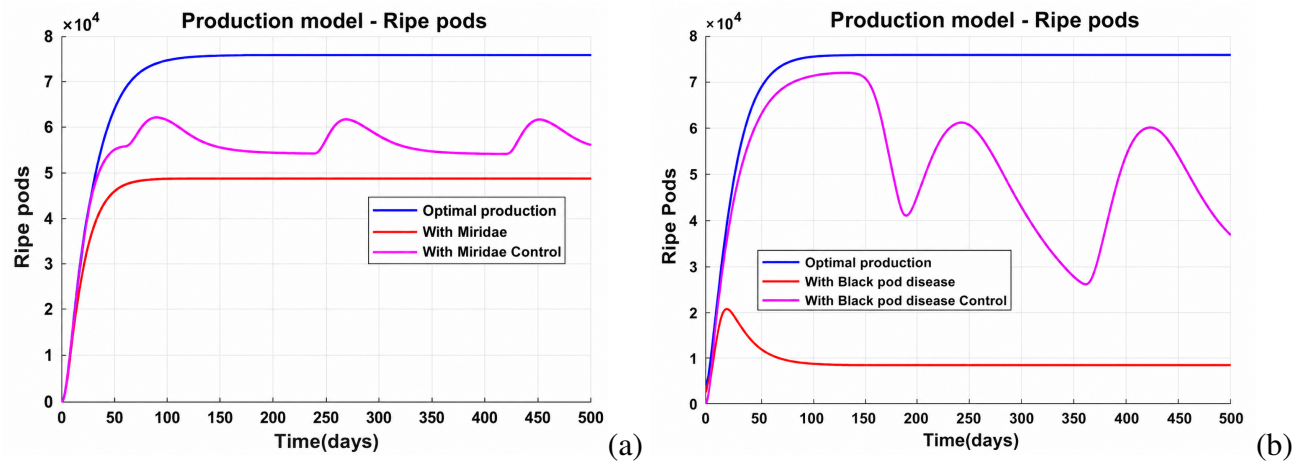


**Figure 19.** Numerical simulation for impulsive control in the plot.

Figure 20 illustrates the outcomes under the different control scenarios. It illustrates the temporal evolution of ripe pods (denoted $S_3$), pods damaged by Miridae (denoted as $I_m$ in the model), infected pods (denoted $I_p$) and co-infected pods (denoted $I_{mp}$) under four distinct control strategies in a cocoa plantation facing both black pod rot disease and Miridae infestation.

- **Magenta curve (no control)**
  In the absence of any intervention, production decreases considerably. Co-infection is devastating; the number of Miridae-damaged pods rises rapidly and remains at a persistently high level. Co-infected pods rise quickly and stay high. The synergy between pests and pathogens is fully expressed. Infected pods rise rapidly to a high endemic level. The disease spreads both via spores and through pest-facilitated infection.
- **Green curve (black pod rot control only – Scenario 1)**
  Production improves slightly but remains very low. Controlling only the disease does little because Miridae continue to damage pods, creating entry points for spores and sustaining the epidemic, almost identical to the magenta curve. Controlling black pod rot does not affect Miridae directly, so damaged pods remain high. This confirms that disease-focused measures alone cannot

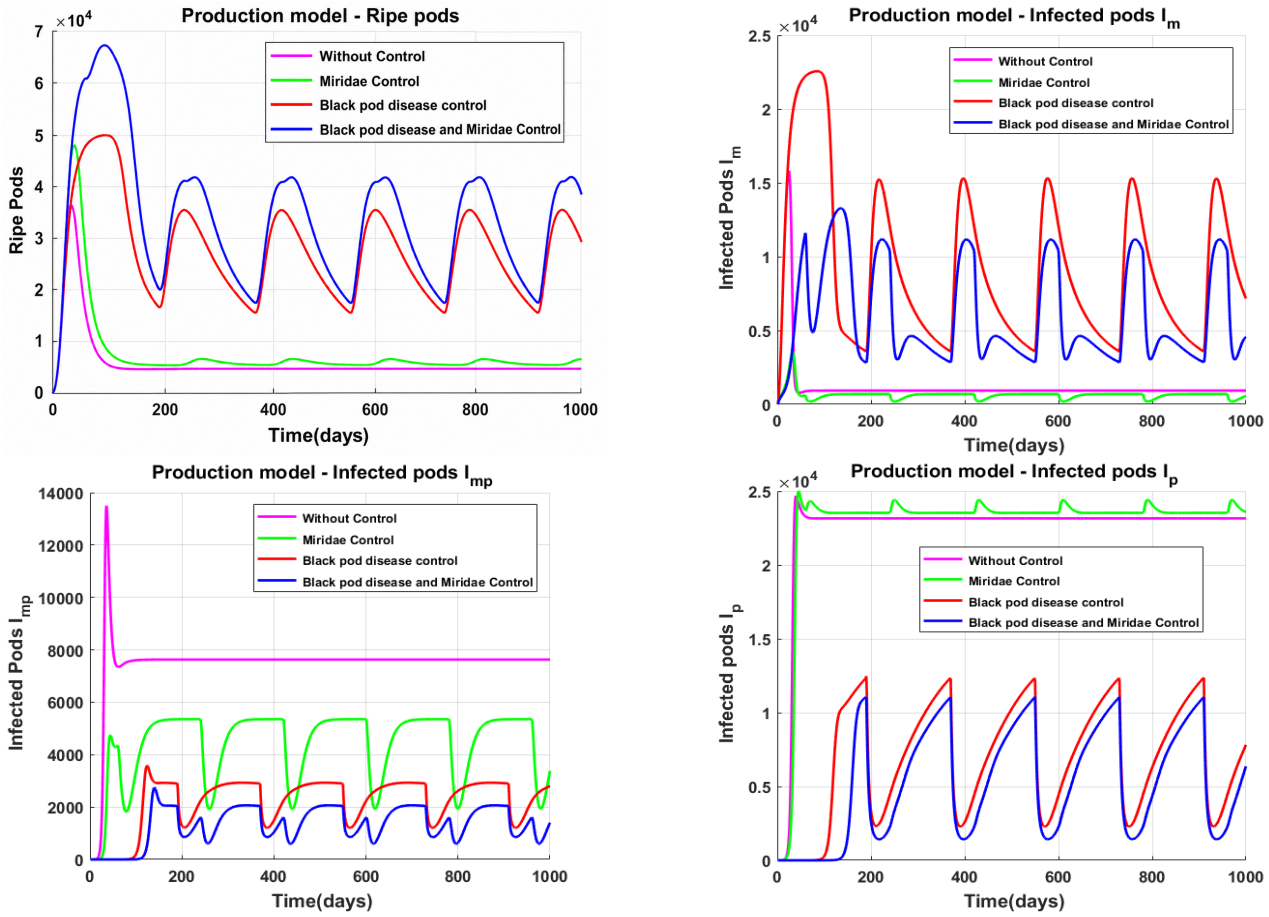


**Figure 20.** Numerical simulations of impulsive control strategies for black pod disease and Miridae. (a) ripe pods; (b) pods damaged by Miridae attacks; (c) co-infected pods; (d) pods infected by black pod disease.

mitigate pest damage. Co-infected pods remain high because Miridae continue to create wounds, and spores can still infect those wounds despite fungicide application (since fungicides target spores but not the wounds themselves). Infected pods are reduced but remain moderate. Fungicides and pod removal lower spore loads and remove infectious material, but Miridae continue to create new infection sites, sustaining the epidemic.

- **Red curve (Miridae control only – Scenario 2)**
  Production improves more significantly but still remains below half of the baseline. Miridae control reduces pod damage, but black pod rot can still spread via direct spore infection of healthy pods. Damaged pods show a periodic sawtooth pattern. Each insecticide application causes an abrupt drop, followed by gradual recovery until the next pulse. The average level is much lower than in the magenta/green curves. Co-infected pods are significantly reduced because fewer Miridae means fewer wounded pods that can become co-infected. However, some co-infection still occurs via direct spore infection of undamaged pods or residual pest activity. Infected pods are also reduced, because fewer Miridae mean fewer wounded pods, reducing one major route of infection. However, direct spore infection of healthy pods can still maintain the disease at a lower level.

**Table 7.** Estimation of production losses under different scenarios.

| | Production without Miridae | Production with Miridae | Production with control | Losses without control | Losses with control |
|---|---|---|---|---|---|
| Ripe pods | 76,000 | 50,000 | 62,000 | 34.21% | 18.42% |
| e | Production without disease | Production with disease | Production with control | Losses without control | Losses with control |
| Ripe pods | 76,000 | 8,400 | 41,600 | 88.94% | 45.26% |
| Co-infection | Production without either threat | Production with co-infection | Production with combi-ned control | Losses without control | Losses with combi-ned control |
| Ripe pods | 76,000 | 5,200 | 35,800 | 93.16% | 52.89% |

- **Blue curve (combined control – Scenario 3)**
  Production reaches the highest level among the co-infection scenarios. The synergy between the two threats is broken by simultaneously reducing both pest damage and disease transmission. Damaged pods are reduced even further than in red. Why? Combined control removes infected pods (which might otherwise remain as resources) and may indirectly reduce Miridae's survival or reproduction through habitat disruption. Co-infected pods drop to the lowest level. Both routes to co-infection (pest-mediated and direct) are suppressed simultaneously. Infected pods reach the lowest level. By simultaneously reducing spores (fungicides), removing infected pods (phytosanitary), and suppressing Miridae (insecticides), the disease is brought under tight control.

Even for a disease like black pod rot, which has its own direct transmission pathway, pest control alone provides significant indirect benefits by closing wound-based infection routes. Combined control maximizes disease suppression. Co-infected pods are a signature of synergistic interaction. Combined control drastically reduces them, breaking the feedback loop where pests create infection sites and disease weakens pods, making them more attractive or vulnerable to pests. Insecticide application (red and blue) effectively reduces Miridae-damaged pods. Combined control achieves the lowest levels, demonstrating that integrated management enhances pest suppression beyond insecticides alone. In co-infected plantations, combined control is far superior to single-threat control. The blue curve demonstrates that integrated management can recover more than half of potential yield, whereas no control leads to total crop failure.

### 3.5.4. Production loss estimates

Table 7 summarizes the production losses (ripe pods) for all scenarios. In this table, we present the estimated production losses for each scenario and compare their outcomes. For each case, production values correspond to the average between the highest and lowest yield peaks. The following table now includes a row for co-infection scenarios with and without combined control.

## 4. Discussion and Conclusion

### *4.1. Summary of the findings*

In this study, we developed and analyzed a deterministic compartmental model to investigate the coupled dynamics of black pod disease and *S. singularis* (Miridae) populations in cocoa plantations. Our primary goal was to quantify production losses under varying pest and disease pressures and evaluate control strategies capable of mitigating their combined impact to optimize yield.

We derived the basic reproduction numbers for each submodel and demonstrated that the DFE is locally asymptotically stable when the reproduction number is below unity. For the spores–pods and Miridae–pods submodels, endemic equilibria were locally stable when the respective reproduction numbers exceeded one. Simulations indicate that, in the absence of an intervention, black pod disease can cause nearly total production loss ($\sim$ 88.94%), while Miridae alone leads to an estimated 34.21% loss. Under co-infection, combined losses exceed 93%, highlighting the synergistic impact of both threats.

### *4.2. Implications of Control Strategies*

To reduce these losses, we implemented impulsive control strategies reflecting practical agricultural practices. Phytosanitary pod removal and fungicide applications target black pod disease, while insecticide spraying controls Miridae populations. Simulations demonstrated substantial improvements under each regime. Two coexistence thresholds were identified: One delineating the persistence of Miridae alone ($\mathcal{N}_0 = 1$), and another marking the transition from coexistence to black pod disease dominance ($\mathcal{R}(\mathcal{Q}_M^*) = 1$). These thresholds provide actionable insights for timing and prioritizing control measures: When $\mathcal{N}_0 > 1$ but $\mathcal{R}(\mathcal{Q}_M^*) < 1$, controlling Miridae alone may be sufficient; when both exceed unity, combined control strategies are necessary.

Our model offers a quantitative framework for integrated pest and disease management in cocoa systems. It supports agronomists and plantation managers in risk assessment, intervention planning, and optimization of control timing and combinations. More broadly, the framework contributes to agroecosystem modeling, demonstrating how coupled pest-disease dynamics shape system's resilience. The identified coexistence thresholds may also serve as early warning indicators of potential regime shifts between pest and disease-dominated states.

### *4.3. Limitations and Future Work*

While the presented loss estimates (Table 7) provide theoretical benchmarks, empirical validation remains essential. Future work should include systematic field data on pod production, infection prevalence, and Miridae's abundance across plantations with known management histories. Such data will enable parameter calibration, enhance predictive accuracy, and strengthen the model's operational relevance.

Several limitations highlight avenues for future research. The model assumes constant environmental conditions and spatial homogeneity, whereas real plantations exhibit variability in microclimate, soil, and pest dispersal. Incorporating stochasticity or spatial structure would improve realism. The current framework focuses solely on black pod disease and Miridae, excluding other pests, pathogens, and ecological interactions that may affect yield. Furthermore, while control strategies improved pro-

duction, the environmental and economic costs were not assessed. Future studies should compare chemical control with sustainable alternatives such as biological control or integrated pest management (IPM). Finally, several parameters were estimated from literature or expert opinion; global sensitivity analysis (e.g., Latin hypercube sampling with PRCCs, as in Marino et al. [27]) is needed to identify which assumed parameters most critically influence production loss estimates. Targeted empirical studies are needed to refine these estimates and test the model under diverse agro-ecological contexts.

### *4.4. Concluding Remarks*

This work represents a first step toward understanding the coupled impact of Miridae and black pod disease through a unified mathematical framework. Although simplified, the model captures key biological processes governing pod development, infection, and pest dynamics in a well-mixed, hectare-scale plantation (approx. 1200 cacao trees producing $\sim$ 14,400 cherelles daily). By explicitly coupling pest–disease interactions with control dynamics, the framework provides a foundation for designing effective management strategies. Future extensions integrating empirical data, stochastic processes, and spatial structure will enhance predictive capacity and decision support, contributing to sustainable cacao production under evolving ecological and economic challenges.

This study demonstrates how a unified theoretical approach can quantify cacao production losses, identify critical coexistence thresholds, and evaluate realistic control strategies. By linking pest–disease dynamics with management interventions, our model provides actionable insights for sustainable agroecosystem management and illustrates the broader value of mathematical ecology in guiding practical decision-making.

## Use of AI tools declaration

The authors declare they have not used Artificial Intelligence (AI) tools in the creation of this article.

## Acknowledgments

The first author is grateful to the Mujeres por Africa Foundation for financial support during the preparation and the finalization of this manuscript. The first author thanks also the Basque Center for Applied Mathematics and especially the Mathematical and Theoretical Biology team for their hospitality, collaboration, and all the logistics provided for the preparation and finalization of this manuscript. M.A. acknowledges the financial support by the Ministerio de Ciencia e Innovación (MICINN) of the Spanish Government through the Ramón y Cajal grant RYC2021-031380-I. This research is also supported by the Basque Government through the BERC 2022-2025 program and by the Spanish Ministry of Sciences, Innovation and Universities: BCAM Severo Ochoa accreditation CEX2021-001142-S / MICIN / AEI / 10.13039/501100011033.

## Conflict of interest

The authors declare there is no conflict of interest.

## References

1. H. Friedel, H. Claudia, K. Irene, M. Pedro, M. Mara, Strengthening the competitiveness of cocoa production and improving the income of cocoa producers in West and Central Africa, *SÜDWIND eV Kaiserstr. Bonn Germany*, **1** (2016), 1–15.
2. B. Duguma, J. Gockowski, J. Bakala, Smallholder cacao (Theobroma cacao Linn.) cultivation in agroforestry systems of West and Central Africa: challenges and opportunities, *Agrofor. Syst.*, **51** (2001), 177–188. https://doi.org/10.1023/A:1010747224249
3. N. Salomon, E. M. I. Bruno, K. B. Ismaël, T. M. D. Denis, C. Christian, Integrated management of Phytophthora diseases on cocoa (Theobroma cacao L): Impact of plant breeding on pod rot incidence, *Crop Protect.*, **26** (2007), 40–45. https://doi.org/10.1016/j.cropro.2006.03.015
4. S. S. Ali, J. Shao, J. L. David, B. A. Kronmiller, D. Y. Shen, M. D. Strem, et al., *Phytophthora megakarya* and *Phytophthora palmivora*, closely related causal agents of cacao black pod rot, underwent increases in genome sizes and gene numbers by different mechanisms, *Genome Biol. Evol.*, **9** (2017), 536–557. https://doi.org/10.1093/gbe/evx021
5. R. Adu-Acheampong, J. Jiggins, A. van Huis, A. R. Cudjoe, V. Johnson, O. Sakyi-Dawson, et al., *The cocoa mirid (Hemiptera: Miridae) problem: evidence to support new recommendations on the timing of insecticide application on cocoa in Ghana*, *Int. J. Trop. Insect Sci.*, **34** (2014), 58–71. https://doi.org/10.1017/S1742758413000441
6. T. M. Djoukwe, B. L. Beilhe, S. Bowong, Y. Dumont, Models for Miridae, a cocoa insect pest. Application in control strategies, *Math. Methods Appl. Sci.*, **41** (2018), 8673–8696. https://doi.org/10.1002/mma.5063
7. T. M. Djoukwe, L. Bagny-Beilhe, Y. Dumont, *Miridae control using sex-pheromone traps. Modeling, analysis and simulations*, *Nonlinear Anal. Real World Appl.*, **54** (2020), 111–119. https://doi.org/10.1016/j.nonrwa.2019.103082
8. C. Nembot, S. P.Takam, G. M. Ten Hoopen, Y. Dumont, Modeling the temporal evolution of cocoa black pod rot disease caused by Phytophthora megakarya, *Math. Methods Appl. Sci.*, **41** (2018), 8816–8843. https://doi.org/10.1002/mma.5206
9. A. Adebayo, O. Adeniyi, A. Olawale, Mathematical model for spread and control of cocoa black pod disease, *Contemp. Math.*, (2023), 549–568. https://doi.org/10.37256/cm.4320233068
10. M. D. Tapi, A. Yakam, R. T. Wafo, S. Bowong, Mathematical modelling and optimal control of production losses caused by Miridae, *Math. Model. Nat. Pheno.*, **18** (2023), 28. https://doi.org/10.1051/mmnp/2023030
11. Entwistle Philip Frank and al. Pests of cocoa. 1972.
12. E. M. Lavabre, J. Decelle, P. Debord, *Recherches sur les variations de populations de mirides (capsides) en Côte d'Ivoire*. Café, Cacao, Thé, **6** (1962), 287–295.
13. Williams G, *Field observations on the cacao mirids, Sahlbergella singularis hagl. and Distantiella theobroma (dist.), in the gold coast. part i. mirid damage*, *Bull. Entomol. Res.*, **44** (1953), 101–119. https://doi.org/10.1017/S0007485300022987
14. V. C. Pence, Abscisic acid in developing zygotic embryos of Theobroma cacao? *Plant Phys.*, **156** (2010), 1291–1293. https://doi.org/10.1104/pp.95.4.1291

15. S. P. Takam, M. Ndoumbè-Nkeng, I. Sache, E. P. Nguema, H. Gwet, J. Chadoeuf, Development stage-dependent susceptibility of cocoa fruit to pod rot caused by Phytophthora megakarya, *Eur. J. Plant Pathol.*, **135** (2013), 363–370. https://doi.org/10.1007/s10658-012-0092-4

16. S. P.Takam, E. P. Nguéma Ndong, H. Gwet, M. Ndoumbè-Nkeng, Smooth estimation of a lifetime distribution with competing risks by using regular interval observations: Application to cocoa fruits growth, *J. Royal Stat. Soc. Ser. C (Appl. Stat.)*, **62** (2013), 741–760. https://doi.org/10.1111/rssc.12019

17. R. Babin, D. H. Bisseleua, L. Dibog, J. P. Lumaret, Rearing method and life-table data for the cocoa mirid bug Sahlbergella singularis Haglund (Hemiptera: Miridae), *J. Appl. Entomol.*, **132** (2008), 366–374. https://doi.org/10.1111/j.1439-0418.2008.01273.x

18. P. Van den Driessche, J. Watmough, Reproduction numbers and sub-threshold endemic equilibria for compartmental models of disease transmission, *Math. Biosci.*, **180** (2002), 29–48. https://doi.org/10.1016/S0025-5564(02)00108-6

19. G. M. Ten Hoopen, P. Deberdt, M. Mbenoun, C. Cilas, Modelling cacao pod growth: Implications for disease control, *Ann. Appl. Biol.*, **160** (2012), 260–272. https://doi.org/10.1111/j.1744-7348.2012.00539.x

20. Y. Dumont, J. Thuilliez, Human behaviors: A threat to mosquito control?, *Math. Biosci.*, **281** (2016), 9–23. https://doi.org/10.1016/j.mbs.2016.08.011

21. B. Drumi, S. Pavel, Impulsive differential equations: Periodic solutions and applications, *Routledge*, (2017).

22. M. Ndoumbe-Nkeng, C. Cilas, E. Nyemb, S. Nyassé, D. Bieysse, A. Flori, et al., Impact of removing diseased pods on cocoa black pod caused by Phytophthora megakarya and on cocoa production in Cameroon, *Crop Protect.*, **23** (2004), 415–424. https://doi.org/10.1016/j.cropro.2003.09.010

23. J. P. LaSalle, The Stability of Dynamical Systems, Society for Industrial and Applied Mathematics, Philadelphia. With an appendix: "Limiting equations and stability of non-autonomous ordinary differential equations" by Z. Artstein, Regional Conference Series in Applied Mathematics, (1976).

24. A. Berman, R. J. Plemmons Robert Nonnegative matrices in the mathematical sciences, (1994). https://doi.org/10.1137/1.9781611971262

25. Ndoumbé Nkeng Michel Incidence des facteurs agro-écologiques sur l'épidémiologie de la pourriture brune des fruits du cacaoyer au Cameroun: contribution à la mise en place d'un modèle d'avertissements agricoles, PhD Thesis, (2002).

26. R. Babin, G. M. Ten Hoopen, C. Cilas, F. Enjalric, P. Gendre, J. Lumaret, et al., Impact of shade on the spatial distribution of Sahlbergella singularis in traditional cocoa agroforests, *Agri. Forest Entomol.*, **12** (2010). https://doi.org/10.1111/j.1461-9563.2009.00453.x

27. S. Marino, I. B. Hogue, C. J. Ray, D. E. Kirschner, A methodology for performing global uncertainty and sensitivity analysis in systems biology, *J. Theor. Biol.*, **254** (2008), 178–196. https://doi.org/10.1016/j.jtbi.2008.04.011

28. B. Y. DHB, V. Stefan, Dispersion models and sampling of cacao mirid bug Sahlbergella singularis

(Hemiptera: Miridae) on Theobroma cacao in Southern Cameroon, *Environ. Entomol.*, **40** (2011), 111–119. https://doi.org/10.1603/EN09101

29. C. Castillo-Chavez, B. Song, Dynamical models of tuberculosis and their applications, *Math. Biosci. Eng.*, **1** (2004), 361–404. https://doi.org/10.3934/mbe.2004.1.361

## Appendix

### A. Derivation of the polynomial

Consider the following system:

$$\begin{cases} \dot{S}_1 &= \Lambda - (\nu + \mu_1 + \alpha)S_1 - \alpha_p S_1 P, \\ \dot{S}_2 &= \nu S_1 - (\gamma + \mu_2)S_2 - \beta_p S_2 P, \\ \dot{I}_p &= \alpha_p S_1 P + \beta_p S_2 P - (\mu_I + \theta)I_p, \\ \dot{P} &= \eta\sigma I_p - \mu_p P. \end{cases} \tag{A.1}$$

From $\dot{S}_1 = 0$, we have

$$S_1(P) = \frac{\Lambda}{\nu + \mu_1 + \alpha + \alpha_p P} = \frac{\Lambda}{\nu + \mu_1 + \alpha + \alpha_p P},$$

From $\dot{S}_2 = 0$, we have

$$S_2(P) = \frac{\nu S_1(P)}{\gamma + \mu_2 + \beta_p P} = \frac{\nu\Lambda}{(\gamma + \mu_2 + \beta_p P)(A + \alpha_p P)},$$

From $\dot{I}_p = 0$, wwe have

$$I_p = \frac{\alpha_p S_1 P + \beta_p S_2 P}{\mu_I + \theta}.$$

From $\dot{P} = 0$, we have

$$I_p = \frac{\mu_p}{\eta\sigma} P.$$

Substituting $(S_1(P))$ and $(S_2(P))$, we have

$$\alpha_p S_1 + \beta_p S_2 = \alpha_p \cdot \frac{\Lambda}{\nu + \mu_1 + \alpha + \alpha_p P} + \beta_p \cdot \frac{\nu\Lambda}{(\gamma + \mu_2 + \beta_p P)(\nu + \mu_1 + \alpha + \alpha_p P)}.$$

Multiply both sides by $(A + \alpha_p P)(B + \beta_p P)$:

$$\alpha_p \Lambda(B + \beta_p P) + \beta_p \nu\Lambda = K(A + \alpha_p P)(B + \beta_p P).$$

Using the two expressions of $I_p$, we have the quadratic equation in $P$:

$$a_2P^2 + a_1P + a_0 = 0, \tag{A.2}$$

where

$$\begin{aligned}
a_2 &= \alpha_p\beta_p\mu_p,\ (\mu_I + \theta),\\
a_1 &= \mu_p\,(\mu_I + \theta)(\beta_p\,(\nu + \mu_1 + \alpha) + \alpha_p\,(\gamma + \mu_2)) - \eta\,\sigma\,\Lambda\,\alpha_p\beta_p,\\
a_0 &= \mu_p\,(\mu_I + \theta)\,(\gamma + \mu_2)\,(\nu + \mu_1 + \alpha)\,(1 - \mathcal{R}^2).
\end{aligned}$$

## B. Proof of Theorem 3

In this appendix, we give the proof of Theorem 3 on the local asymptotic stability of the endemic equilibrium $\overline{Q}$ of the spores–pods model. We first recall the theorem of Castillo-Chavez and Song [29].

**Theorem 6.** *(Castillo-Chavez and Song [29]) Let*

$$\frac{dx}{dt} = f(x,\phi), \quad f : \mathbb{R}^n \times \mathbb{R} \longleftrightarrow \mathbb{R}^n \text{ and } f \in C^2(\mathbb{R}^n \times \mathbb{R}). \tag{B.1}$$

*Without loss of generality, it is assumed that* $\mathbf{0}$ *is a trivial equilibrium for System (B.1) for all values of the parameter* $\phi$*, that is*

$$f(0,\phi) \equiv 0 \text{ for all } \phi. \tag{B.2}$$

*Assume*

$A_1$ $A = D_x f(\mathbf{0}) = \left(\dfrac{\partial f_i}{\partial x_j}(\mathbf{0})\right)$ *is the linearisation matrix of System (B.1) around the equilibrium* $\mathbf{0}$ *with* $\phi$ *evaluated at* 0*. Zero is a simple eigenvalue of A and all other eigenvalues of A have negative real parts;*

$A_2$ *Matrix A has a non-negative right eigenvector w and a left eigenvector v corresponding to the zero eigenvalue.*

*Let* $f_k$ *be the kth component of* $f$ *and*

$$a_1 = \sum_{k,i,j=1}^{n} v_k w_i w_j \frac{\partial^2 f_k}{\partial x_i \partial x_j}(\mathbf{0}) \tag{B.3}$$

$$b_1 = \sum_{k,i=1}^{n} v_k w_i \frac{\partial^2 f_k}{\partial x_i \partial \phi}(\mathbf{0}) \tag{B.4}$$

*The local dynamics of System (B.1) around* $\mathbf{0}$ *are totally determined by* $a_1$ *and* $b_1$ *as follows.*

*(i)* $a_1 > 0$, $b_1 > 0$. *When* $\phi < 0$ *with* $|\phi| \ll 1$, $\mathbf{0}$ *is locally asymptotically stable, and there is a positive unstable equilibrium; when* $0 < \phi \ll 1$, $\mathbf{0}$ *is unstable and thereis a negative and locally asymptotically stable equilibrium;*

*(ii)* $a_1 < 0$, $b_1 < 0$. *When* $\phi < 0$ *with* $|\phi| \ll 1$, $\mathbf{0}$ *is unstable; when* $0 < \phi \ll 1$, $\mathbf{0}$ *is locally asymptotically stable, and there is a positive unstable equilibrium;*

*(iii)* $a_1 > 0$, $b_1 < 0$. *When* $\phi < 0$ *with* $|\phi| \ll 1$, $\mathbf{0}$ *is unstable, and there is a locally asymptotically stable negative equilibrium; when* $0 < \phi \ll 1$, $\mathbf{0}$ *is stable, and a positive unstable equilibrium appears;*

*(iv)* $a_1 < 0$, $b_1 > 0$. *When* $\phi$ *changes from negative to positive,* $\mathbf{0}$ *changes its stability from stable to unstable. Correspondingly, a negative unstable equilibrium becomes positive and locally asymptotically stable.*

*Particularly, if* $a_1 > 0$ *and* $b_1 > 0$, *then a backward bifurcation occurs at* $\phi = 0$.

To study the stability of the endemic equilibria $\overline{Q}$ around $\mathcal{R}$, we use Theorem 6. We first introduce a positive parameter $\eta$. Solving $\mathcal{R} = 1$ gives

$$\eta = \eta^* = \frac{\mu_p\,(\mu_I + \theta)\,(\gamma + \mu_2)\,(\nu + \mu_1 + \alpha)}{\sigma\,\Lambda\,(\beta_p\,\nu + \alpha_p\,(\gamma + \mu_2))}.$$

To apply this theory, the following simplifications and change of variables are made. Let $x_1 = S_1$, $x_2 = S_2$, $x_3 = I_p$, and $x_4 = P$. Moreover, by using the vector notation $x = (x_1, x_2, x_3, x_4)$, System (3.3) can be written in the form $\dot{x} = f(x)$, with $f = (f_1, f_2, f_3, f_4)$, as follows:

$$\begin{cases} \dot{x}_1 = f_1 = \Lambda - (\nu + \mu_1 + \alpha)\,x_1 - \alpha_p\,x_1\,x_4, \\ \dot{x}_2 = f_2 = \nu\,x_1 - (\gamma + \mu_2)\,x_2 - \beta_p\,x_2\,x_4, \\ \dot{x}_3 = f_3 = (\alpha_p\,x_1 + \beta_p\,x_2)\,x_4 - (\mu_I + \theta)\,x_3, \\ \dot{x}_4 = f_4 = \eta\,\sigma\,x_3 - \mu_p\,x_4. \end{cases} \tag{B.5}$$

The Jacobian matrix around the DFE $Q^0$ when $\eta = \eta^*$ is given by

$$J(Q^0) = \begin{pmatrix} -(\nu + \mu_1 + \alpha) & 0 & 0 & -\alpha_p\,S_1^0 \\ \nu & -(\gamma + \mu_2) & 0 & -\beta_p\,S_2^0 \\ 0 & 0 & -(\mu_I + \theta) & \alpha_p\,S_1^0 + \beta_p\,S_2^0 \\ 0 & 0 & \eta^*\,\sigma & -\mu_p \end{pmatrix}.$$

**Eigenvectors of** $J(Q^0)$: The Jacobian $J(Q^0)$ has a right eigenvector (corresponding to the zero eigenvalue), given by $u = (u_1, u_2, u_3, u_4)^T$, where

$$\begin{cases} u_1 = -\left(\dfrac{\alpha_p\,S_1^0}{\nu + \mu_1 + \alpha}\right)u_4, \\ u_2 = -\left(\dfrac{\beta_p\,S_2^0}{\gamma + \mu_2} + \dfrac{\nu\,\alpha_p\,S_1^0}{(\nu + \mu_1 + \alpha)(\gamma + \mu_2)}\right)u_4, \\ u_3 = \left(\dfrac{\alpha_p\,S_1^0 + \beta_p\,S_2^0}{\mu_I + \theta}\right)u_4, \\ u_4 = u_4 > 0. \end{cases}$$

Similarly, the components of the left eigenvector of $J(Q^0)$ (corresponding to the zero eigenvalue), denoted $v = (v_1, v_2, v_3, v_4)$, are given by

$$\begin{cases} v_1 = v_2 = 0, \\ v_3 = \left(\dfrac{\mu_p}{\alpha_p S_1^0 + \beta_p S_2^0}\right) v_4, \\ v_4 = v_4 > 0. \end{cases}$$

**Computation of** $a_1$: For System (B.5), the associated non-zero partial derivatives of $f$ (at the DFE) are given by:

$$\frac{\partial^2 f_1}{\partial x_1 \partial x_4} = \frac{\partial^2 f_1}{\partial x_4 \partial x_1} = -\alpha_p, \quad \frac{\partial^2 f_2}{\partial x_2 \partial x_4} = \frac{\partial^2 f_2}{\partial x_4 \partial x_2} = -\beta_p, \quad \frac{\partial^2 f_3}{\partial x_1 \partial x_4} = \frac{\partial^2 f_3}{\partial x_4 \partial x_1} = \alpha_p,$$

$$\text{and} \qquad \frac{\partial^2 f_3}{\partial x_2 \partial x_4} = \frac{\partial^2 f_3}{\partial x_4 \partial x_2} = \beta_p.$$

Then

$$\begin{aligned} a_1 &= v_3 \sum_{i,j=1}^{4} u_i u_j \frac{\partial^2 f_3(Q^0)}{\partial x_i \partial x_j} \\ &= -2\, u_4 \left( \frac{\alpha_p^2 S_1^0}{\nu + \mu_1 + \alpha} + \beta_p \left( \frac{\beta_p S_2^0}{\gamma + \mu_2} + \frac{\nu\, \alpha_p S_1^0}{(\nu + \mu_1 + \alpha)(\gamma + \mu_2)} \right) \right) < 0. \end{aligned}$$

**Computation of** $b_1$: For the sign of $b_1$, it can be shown that the associated non-vanishing partial derivatives of $f$ are:

$$\frac{\partial^2 f_4}{\partial x_3 \partial \eta}(Q^0) = \sigma.$$

Substituting the respective partial derivatives into the expression gives

$$b_1 = v_4\, \sigma \left( \frac{\alpha_p S_1^0 + \beta_p S_2^0}{\mu_I + \theta} \right) u_4 > 0.$$

Thus, $a_1 < 0$ and $b_1 > 0$. This corresponds to Case (iv) of Theorem 6: When $\mathcal{R}$ crosses 1 from below, the DFE changes stability from stable to unstable, and a positive (endemic) equilibrium emerges that is locally asymptotically stable. This completes the proof of Theorem 3. □

## C. Proof of Theorem 5

We prove that when $\mathcal{N}_0 \geq 1$, the unique endemic equilibrium of System (3.10) is locally asymptotically stable. The proof is based on the bifurcation theorem of Castillo-Chavez and Song [29], which establishes the direction of the transcritical bifurcation at $\mathcal{N}_0 = 1$ and the local stability of the endemic equilibrium for $\mathcal{N}_0 > 1$.

The pest-free equilibrium (DFE) is $\xi^0 = \left(S_1^0, S_2^0, 0, 0, 0\right)$. We choose $b$ as the bifurcation parameter. The critical value where $\mathcal{N}_0 = 1$ is

$$b^0 = \frac{\mu_m (\nu_E + \mu_E)}{r\, \nu_E}.$$

The Jacobian matrix $J = Df(\xi_0, b^0)$ has a simple zero eigenvalue. Order the variables as $(S_1, S_2, I_m, E, M)$. We then have

$$J = \begin{pmatrix} -(\nu+\mu_1+\alpha) & 0 & 0 & 0 & -\alpha_m S_1^0 \\ \nu & -(\gamma+\mu_2) & 0 & 0 & -\beta_m S_2^0 \\ 0 & 0 & -\mu_I & 0 & \alpha_m S_1^0 + \beta_m S_2^0 \\ 0 & 0 & 0 & -(\nu_E+\mu_E) & rb^0 \\ 0 & 0 & 0 & \nu_E & -\mu_m \end{pmatrix}.$$

Let $\mathbf{v}$ be the right eigenvector for zero eigenvalue. Solve $J\mathbf{v} = 0$, with $\mathbf{v} = (v_1, v_2, v_3, v_4, v_5)^T$, we find

$$\mathbf{v} = \left( -\frac{\alpha_m S_1^0}{\nu+\mu_1+\alpha}, \quad \frac{\nu\alpha_m S_1^0}{\gamma+\mu_2} + \frac{\beta_m S_2^0}{(\gamma+\mu_2)(\nu+\mu_1+\alpha)}, \quad \frac{\alpha_m S_1^0 + \beta_m S_2^0}{\mu_I}, \quad \frac{rb}{\nu_E^0+\mu_E}, 1 \right)$$

Let $\mathbf{w}$ be the left eigenvector for zero eigenvalue. Solve $\mathbf{w}J = 0$, with $\mathbf{w} = (w_1, w_2, w_3, w_4, w_5)$, we find

$$\mathbf{w} = \left( 0,\ 0,\ 0,\ \frac{\nu_E}{\nu_E+\mu_E},\ 1 \right).$$

**Computation of coefficient $a_1$**

The coefficient $a_1$ is given by:

$$a_1 = \sum_{k,i,j=1}^{5} w_k v_i v_j \frac{\partial^2 f_k}{\partial x_i \partial x_j}(\xi^0, b^0).$$

Since $w_1 = w_2 = w_3 = 0$, we only use the equation for $\dot{E}$) and $k = 5$ as the equation for $\dot{M}$.
After computation, we find

$$a_1 = -\frac{2\mu_m r b^0}{K(\nu_E+\mu_E)} + \frac{2ed(\alpha_m S_1^0 + \beta_m S_2^0)}{\mu_I}.$$

**Computation of coefficient $b_1$ (with respect to bifurcation parameter $\phi = b_1$)**

The coefficient $b_1$ is given by:

$$b_1 = \sum_{k,i=1}^{5} w_k v_i \frac{\partial^2 f_k}{\partial x_i \partial b}(\xi^0, b^0).$$

We only need the term where $f_4$ (the equation for $\dot{E}$). The parameter $b$ appears only in the equation for $\dot{E}$.
After computation, we find

$$b_1 = \frac{r\nu_E}{\nu_E+\mu_E} > 0.$$

We have:

$$a_1 = -\frac{2\mu_m r b^0}{K(\nu_E+\mu_E)} + \frac{2ed(\alpha_m S_1^0 + \beta_m S_2^0)}{\mu_I}, \quad b = \frac{r\nu_E}{\nu_E+\mu_E} > 0.$$

Since $b > 0$ always, and typically $a < 0$ for certain values. In that case, we are in **Case (iv)** of the Castillo-Chavez and Song theorem. This implies that: when $b$ increases through $b^0$ (i.e., $\mathcal{N}_0$ increases through 1), the DFE changes stability from stable to unstable, a positive endemic equilibrium appears for $b > b^0$ ($\mathcal{N}_0 > 1$) and is locally asymptotically stable. This completes the proof of Theorem 5. □